Received: 8 June 2020 | Accepted: 4 October 2020

DOI: 10.1002/vzj2.20083

Vadose Zone Journal

ORIGINAL RESEARCH ARTICLE

A profile shape correction to reduce the vertical sensitivity of cosmic-ray neutron sensing of soil moisture

Lena M. Scheiffele[1] | **Gabriele Baroni**[2] | **Trenton E. Franz**[3] | **Jannis Jakobi**[4] | **Sascha E. Oswald**[1]

[1] Institute of Environmental Science and Geography, Univ. of Potsdam, Karl-Liebknecht-Str. 24-25, Potsdam 14476, Germany

[2] Dep. of Agricultural and Food Sciences, Univ. of Bologna, Viale Fanin 50, Bologna, Italy

[3] School of Natural Resources, Univ. of Nebraska–Lincoln, 303 South Hardin Hall, 3310 Holdrege St., Lincoln, NE 68583-0973, USA

[4] Forschungszentrum Jülich, Agrosphere Institute (IBG-3), Jülich 52425, Germany

Correspondence
Lena M. Scheiffele, Institute of Environmental Science and Geography, Univ. of Potsdam, Karl-Liebknecht-Str. 24-25, 14476 Potsdam, Germany.
Email: lena.scheiffele@uni-potsdam.de

Assigned to Associate Editor Scott Jones.

Funding information
Deutsche Forschungsgemeinschaft, Grant/Award Number: FOR-2694

Abstract

In recent years, cosmic-ray neutron sensing (CRNS) has shown a large potential among proximal sensing techniques to monitor soil moisture noninvasively, with high frequency and a large support volume (radius up to 240 m and sensing depth up to 80 cm). This signal is, however, more sensitive to closer distances and shallower depths. Inherently, CRNS-derived soil moisture is a spatially weighted value, different from an average soil moisture as retrieved by a sensor network. In this study, we systematically test a new profile shape correction on CRNS-derived soil moisture, based on additional soil moisture profile measurements and vertical unweighting, which is especially relevant during pronounced wetting or drying fronts. The analyses are conducted with data collected at four contrasting field sites, each equipped with a CRNS probe and a distributed soil moisture sensor network. After applying the profile shape correction on CRNS-derived soil moisture, it is compared with the sensor network average. Results show that the influence of the vertical sensitivity of CRNS on integral soil moisture values is successfully reduced. One to three properly located profile measurements within the CRNS support volume improve the performance. For the four investigated field sites, the RMSE decreased 11–53% when only one profile location was considered. We therefore recommend to install along with a CRNS at least one soil moisture profile in a radial distance <100 m and a measurement depth down to 50 cm. Profile-shape-corrected, CRNS-derived soil moisture is an unweighted integral soil moisture over the support volume, which is easier to interpret and easier to use for further applications.

1 | INTRODUCTION

Soil moisture is an important hydrological state variable to assess the energy balance and the partitioning of hydrologic fluxes at the land surface (Corradini, 2014). For this reason, there are wide hydrologic applications for soil moisture data (Brocca, Ciabatta, Massari, Camici, & Tarpanelli, 2017).

ABBREVATIONS: AHP, additional hydrogen pools; CRNS, cosmic-ray neutron sensing; HOAL, Hydrological Open Air Laboratory; KAT, Katharinentaler Hof; KGE, Kling–Gupta efficiency; MAE, mean absolute error; NSE, Nash–Sutcliffe efficiency; SEL, Selhausen; SRER, Santa Rita Experimental Range.

This is an open access article under the terms of the Creative Commons Attribution License, which permits use, distribution and reproduction in any medium, provided the original work is properly cited.
© 2020 The Authors. *Vadose Zone Journal* published by Wiley Periodicals LLC on behalf of Soil Science Society of America

Antecedent soil moisture states are used for flood and landslide forecasting (Brocca et al., 2012; Koster, Mahanama, Livneh, Lettenmaier, & Reichle, 2010) and to study the interactions in soil–atmosphere processes (Seneviratne et al., 2010). The soil moisture state is important for drought prediction (Pendergrass et al., 2020) and can be decisive for the occurrence of heat waves (Wehrli, Guillod, Hauser, Leclair, & Seneviratne, 2019). Irrigated agriculture can especially benefit from soil moisture monitoring data (Barker, Franz, Heeren, Neale, & Luck, 2017; Finkenbiner, Franz, Gibson, Heeren, & Luck, 2019). Hydrologic and land surface models require the input of intermediate scale soil moisture data of the integrated active layer (Shrestha & Simmer, 2020).

In the last decade, cosmic-ray neutron sensing (CRNS) has evolved to a well-established, noninvasive method for monitoring soil moisture at high temporal resolution (hourly to daily values), and it is now applied in several monitoring networks and at many research stations around the world (Andreasen, Jensen, Desilets, Zreda, et al., 2017; Baatz et al., 2014; Evans et al., 2016; Fersch et al., 2020; Hawdon, McJannet, & Wallace, 2014; Zreda et al., 2012). Cosmic-ray neutron sensing uses the natural occurring background neutron flux and its inverse proportional relationship with hydrogen abundance (present mainly as soil moisture) at the land surface (Zreda, Desilets, Ferré, & Scott, 2008; Zreda et al., 2012). Its outstanding features are the noninvasive installation aboveground and the large support volume with a radius of ≥150 m around the sensor and integration depth of 12–80 cm (Köhli et al., 2015; Schrön et al., 2017). Because of these features, CRNS proves to be useful for soil moisture monitoring at the field scale and in validating remote sensing products (Duygu & Akyürek, 2019; Montzka et al., 2017).

Cosmic-ray neutron sensing has been successfully applied in contrasting environments, ranging from drylands (Franz, Zreda, Rosolem, & Ferre, 2012) to temperate humid conditions (Baatz et al., 2014), forests (Andreasen, Jensen, Desilets, Franz, et al., 2017; Bogena, Huisman, Baatz, Hendricks Franssen, & Vereecken, 2013; Heidbüchel, Güntner, & Blume, 2016), and urban areas (Schrön, Zacharias, et al., 2018). In addition to fixed installation, it can also be used in mobile applications (Chrisman & Zreda, 2013; Dong, Ochsner, Zreda, Cosh, & Zou, 2014; Fersch, Jagdhuber, Schrön, Völksch, & Jäger, 2018; Jakobi, Huisman, Vereecken, Diekkrüger, & Bogena, 2018; Jakobi et al., 2020; Schrön, Rosolem, et al., 2018). Because of its noninvasive installation, it is especially suited for agricultural field sites (Barker et al., 2017; Baroni & Oswald, 2015; Finkenbiner et al., 2019; Franz, Wang, Avery, Finkenbiner, & Brocca, 2015; Jakobi et al., 2018; McJannet, Hawdon, Baker, Renzullo, & Searle, 2017; Ragab, Evans, Battilani, & Solimando, 2017; Rivera Villarreyes, Baroni, & Oswald, 2011; Wang et al., 2018), as traditional point sensors often have to be removed during management operations. At the field scale, CRNS delivers an integrated value of soil moisture, whereas a large number of point sensors is needed to deliver a comparable result, overcoming small-scale heterogeneity within the field (Ochsner et al., 2013; Robinson et al., 2008; Teuling, Uijlenhoet, Hupet, van Loon, & Troch, 2006). For better understanding and validation of the CRNS signal, many studies tested the performance of CRNS in comparison with networks of point sensors, which can reach a similar extent to the CRNS support volume (Baatz et al., 2014; Baroni, Scheiffele, Schrön, Ingwersen, & Oswald, 2018; Bogena et al., 2013; Franz, Zreda, Rosolem, & Ferre, 2012; Franz et al., 2016; Iwema, Rosolem, Baatz, Wagener, & Bogena, 2015; Jakobi et al., 2018; Schreiner-McGraw, Vivoni, Mascaro, & Franz, 2016).

A drawback of the CRNS method within this comparison is the higher sensitivity to upper soil layers and closer distances. This needs to be considered during calibration of the sensor and when comparing soil moisture time series. Early studies set up sensor networks with locations representing the exponential decrease in sensitivity with distance from the CRNS, which made a horizontal weighting unnecessary (Franz, Zreda, Rosolem, & Ferre, 2012; Zreda et al., 2012), and even better comparability could be achieved when the point sensors were vertically weighted (Franz, Zreda, Ferre, et al., 2012). Early on it was recognized that better calibration results are achieved when other hydrogen pools are considered (e.g., water in the crystal lattice of minerals or water equivalent stored in soil organic material, see Hawdon et al., 2014; Zreda et al., 2012). Köhli et al. (2015) and Schrön et al. (2017) further improved the understanding of the sensitivity of the sensor with the help of neutron transport modeling. They refined the procedures of vertical and horizontal weighting of point soil moisture information to better mimic the signal detected by CRNS. Therefore, CRNS represents a weighted total water content, which hinders its easy interpretation and use for application in hydrologic models and other practical data products (Franz et al., 2020). For data assimilation purposes, the COSMIC operator was developed (Shuttleworth, Rosolem, Zreda, & Franz, 2013), which deals with the inherent weighting by directly using the neutron counts and not the

Core Ideas

- Soil moisture derived from cosmic-ray neutron sensing is inherently weighted.
- Few additional soil moisture profile measurements should complement the method.
- A profile shape correction unweights cosmic-ray-derived soil moisture.
- Corrected cosmic-ray soil moisture is a better integral average of the support volume.

CRNS-derived soil moisture. Different studies tried to tackle the problem by extending the measurement depth of CRNS to the root zone with the use of an exponential filter (Dimitrova-Petrova et al., 2020; Franz et al., 2020; Peterson, Helgason, & Ireson, 2016), or merging CRNS information with data from point sensors of deeper layers (Nguyen, Jeong, & Choi, 2019). However, they assumed CRNS to be representative for the upper most soil layer (down to 15-to-30-cm depth) and did not specifically consider the decreasing sensitivity with depth.

A previous study assessed the uncertainty in CRNS-derived soil moisture when compared with an unweighted sensor network (Baroni et al., 2018). It was found that the sensitivity of CRNS on the depth-dependent distribution of soil moisture was an important source of uncertainty, increasing with pronounced wetting or drying fronts within the profile. This was also assessed with numerical tests and synthetic derived soil moisture profiles. Based on this finding, a simple profile shape correction to apply on CRNS-derived soil moisture was outlined there, which reduces the influence of the vertical sensitivity. The profile shape correction includes an "unweighting" of CRNS-derived soil moisture by using the vertical weighting of point soil moisture measurements. Profile-shape-corrected, CRNS-derived soil moisture should then be better representative of the volumetric average soil moisture within the support volume. To apply such a correction, CRNS measurements need to be accompanied by installation of additional soil moisture profile measurements. As this is a drawback in terms of noninvasive installation, the question arises how to best install additional point sensors to balance installation effort and performance with the profile shape correction. An ideal location would be the one representative of the areal mean soil moisture, as could be identified by using the concept of temporal stable soil moisture locations (Vereecken et al., 2014). There are studies comparing CRNS with temporal stable soil moisture locations (Nguyen, Kim, & Choi, 2017; Nguyen et al., 2019; Peterson et al., 2016; Zhu et al., 2017). However, these locations cannot be determined beforehand (Vanderlinden et al., 2012), and the methods are therefore less feasible for the use of CRNS as a soil moisture monitoring method.

In our study, we systematically test the application of the profile shape correction (developed based on results from numerical tests) on comprehensive experimental datasets and address issues that arise with it: (a) do we improve CRNS-derived integral soil moisture by a procedure correcting for the profile shape, in comparison with a sensor network; (b) how many additional soil moisture profiles would be required to achieve satisfactory results; (c) down to which depth and (d) at which distance from CRNS should the additional measurements be installed? Additionally, we test different vertical weighting options. To address these questions, we use data from four field sites, where a sensor network and CRNS were operated simultaneously. The field sites show pronounced differences in soil and climatic conditions, absolute values of their soil moisture regimes, and setup of sensor networks and thus provide a broad basis for testing the procedure.

2 | MATERIALS AND METHODS

2.1 | From neutron counts to soil moisture

The neutrons measured by the CRNS sensor are generated as part of a secondary particle cascade from cosmic radiation. Hydrogen is the element most effective in moderating neutrons of this specific energy range (~1 MeV), and at the land surface it is mostly present as soil moisture. Neutrons entering the soil are moderated to lower energy levels and partly reflected back to the atmosphere. Thus, an inverse relationship between neutrons detected aboveground and the soil moisture can be established (Desilets, Zreda, & Ferré, 2010; Zreda et al., 2008). Due to the interaction physics of neutrons, the neutrons are traveling at very high velocities and mix nearly instantaneously within the air horizontally above the soil and also probe deeper soil layers. This leads to the large support volume of the sensor of up to 240-m radius and an effective measurement depth of up to 80 cm in dry soils (for details, see Köhli et al., 2015; Zreda et al., 2012). Cosmic-ray neutrons are sensitive to changes in atmospheric pressure, absolute humidity, and incoming cosmic radiation. In this study, we applied those three standard correction procedures, which can be found in Appendix A.

The corrected neutron counts can be converted to soil moisture (θ_{CRNS}, $m^3\ m^{-3}$) following the calibration proposed by Desilets et al. (2010), for volumetric water content (Rivera Villarreyes et al., 2011):

$$\theta_{CRNS} = \left(\frac{a_0}{N/N_0 - a_1} - a_2 \right) \frac{\rho_b}{\rho_w} \quad (1)$$

where ρ_b and ρ_w are the soil bulk density ($g\ cm^{-3}$) and the density of water (assumed to be 1 $g\ cm^{-3}$), respectively; a_i have been derived from neutron simulations and are usually kept constant ($a_0 = 0.0808$, $a_1 = 0.372$, and $a_2 = 0.115$), whereas N_0 is the single site-specific parameter to be calibrated.

As the sensor is sensitive not only to soil moisture but to all hydrogen within its support volume, better results can be achieved when additional hydrogen pools are accounted for in the calibration (Hawdon et al., 2014). In soil, hydrogen is stored in organic matter and within the crystal lattice of clay minerals (for details about measurements and calculations, refer to Appendix B). These pools can be assumed static for the timescale of soil moisture observations dealt with in

this study and are combined to one pool of additional soil hydrogen pools (AHP, $m^3\ m^{-3}$). Also, hydrogen in biomass is important to consider when using CRNS (Baatz et al., 2015; Baroni & Oswald, 2015; Coopersmith, Cosh, & Daughtry, 2014; Franz, Zreda, Rosolem, Hornbuckle, et al., 2013; Jakobi et al., 2018). For this study, we neglect the influence of biomass change as it is a small water pool within the footprint compared with soil moisture. Research on how to include biomass influence in calibration or correction of the CRNS signal is ongoing (see Franz et al., 2015, for corrections on N_0 for growing maize [*Zea mays* L.] and soybeans [*Glycine max* (L.) Merr.]) but can be easily implemented in the correction framework proposed here, once a standard is established.

2.2 | Horizontal and vertical sensitivity of the signal

The CRNS signal is more sensitive to areas closer to the detector and to shallower soil depths. In early studies, the horizontal placing of calibration locations was chosen to represent the horizontal exponential decrease in sensitivity. For the vertical sensitivity, a weighting procedure was introduced (Franz, Zreda, Ferre, et al., 2012), calculating the weights for each depth as follows:

$$\mathrm{wt}\,(d) = a\left[1 - \left(\frac{d}{d^*}\right)^b\right] \tag{2a}$$

$$a = 1\Big/\left\{d^* - \left[\frac{d^{*b+1}}{d^{*b}\,(b+1)}\right]\right\} \tag{2b}$$

with d being the depth (cm), and b being 1 for a linear weighting. d^* (cm) is the effective measurement depth of the sensor (86% of neutrons detected by the sensor originate from above this depth) determined as

$$d^* = \frac{5.8}{\theta_{\mathrm{tot}} + \mathrm{AHP} + 0.0829} \tag{3}$$

where θ_{tot} ($= \theta_{\mathrm{v}} + \mathrm{AHP}$) is the total water content including volumetric soil moisture (θ_{v}, from calibration soil samples or an accompanying sensor network) and additional hydrogen pools (AHP, Franz, Zreda, Rosolem, & Ferre, 2013).

More recently, Köhli et al. (2015) and Schrön et al. (2017) revised the understanding of the support volume properties and adjusted the weighting functions. The vertical weights follow an exponential decrease:

$$\mathrm{wt}\,(d) = e^{-2d/D_{86}} \tag{4}$$

where the effective penetration depth D_{86} (cm) is dependent on the distance of the location to the CRNS expressed as rescaled radius r^* (dependent on air pressure, absolute humidity, and vegetation height; Appendix C):

$$D_{86} = \rho_{\mathrm{b}}^{-1}\left[p_0 + p_1\left(p_2 + e^{p_3 r^*}\right)\frac{p_4 + \theta_{\mathrm{tot}}}{p_5 + \theta_{\mathrm{tot}}}\right] \tag{5}$$

for parameter values refer to Schrön et al. (2017).

For both vertical weighting methods the resulting water content is calculated by

$$\theta_{\mathrm{tot(wt)}} = \frac{\sum \theta_{\mathrm{tot}} \cdot \mathrm{wt}}{\sum \mathrm{wt}} \tag{6}$$

This is also represented in the calibration function as follows:

$$\theta_{\mathrm{CRNS}} = \theta_{\mathrm{tot(wt)}} = \left(\frac{a_0}{N/N_0 - a_1} - a_2\right)\frac{\rho_{\mathrm{b}}}{\rho_{\mathrm{w}}} \tag{7}$$

with $\theta_{\mathrm{tot(wt)}} = (\theta_{\mathrm{v}} + \mathrm{AHP})_{\mathrm{wt}}$ and θ_{CRNS} also representing a total weighted water content. These two options for the vertical weighting will also be compared within our study and will be called D_{F} (following Franz, Zreda, Ferre, et al., 2012) and D_{K} (following Köhli et al., 2015) hereafter.

The complete weighting procedure for point soil moisture data as proposed by Köhli et al. (2015) and Schrön et al. (2017) further includes a horizontal weighting (Appendix C). This weighting leads to an improved estimate of the spatial sensitivity of the sensor (Cai, Pang, & Fu, 2018). Considering additional hydrogen pools and applying a weighting on soil samples delivers best calibration results. Point measurements from a sensor network can also be used to assess CRNS (e.g., simply to compare time series dynamics, to calibrate CRNS with sensor network data, and to determine CRNS support volume). For this reason, these two steps should also be applied to point measurements from distributed sensor networks when compared with CRNS-derived soil moisture (Schrön et al., 2017).

For comparing CRNS-derived soil moisture with other soil moisture measurements, the bias introduced by the included AHP is widely recognized, and within many studies, AHP are subtracted from CRNS-derived soil moisture after proper calibration (Hawdon et al., 2014; Jakobi et al., 2018) to derive a "volumetric" CRNS-derived soil moisture and thus better comparability with a standard average from a sensor network. The inherent weighting, however, is not treated within these experimental studies.

Within the present study, θ_{CRNS} represents a total weighted water content as best calibration result. The bias of the AHP contained in θ_{CRNS} is considered within the profile shape correction.

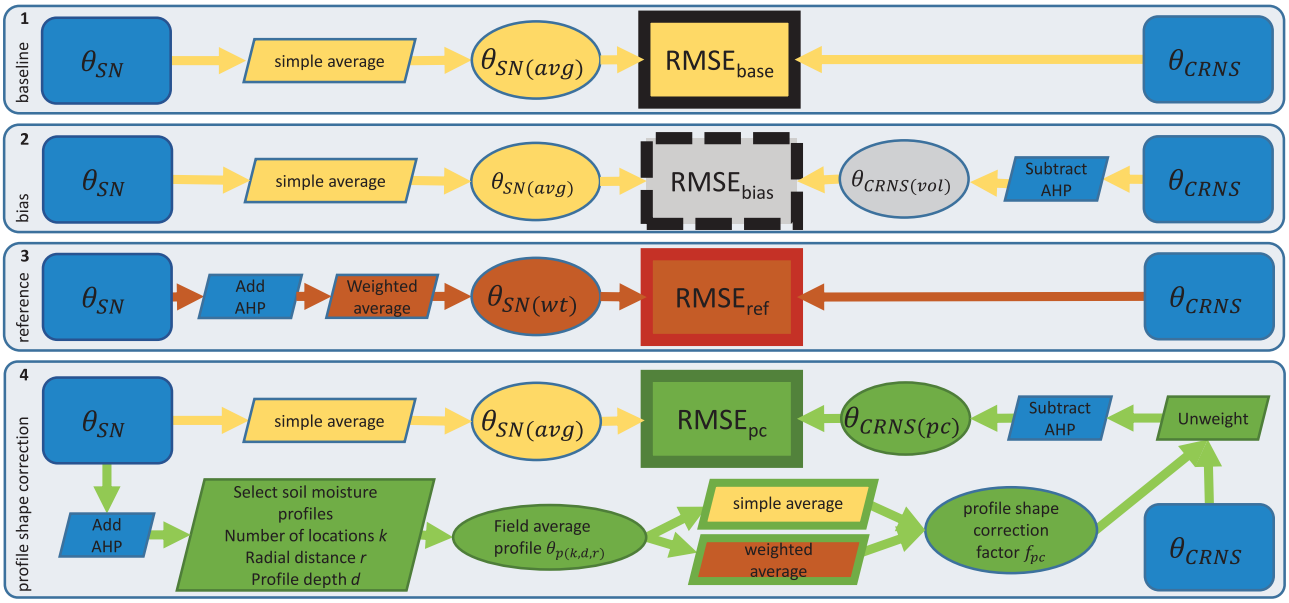

FIGURE 1 Different options to compare soil moisture from the distributed sensor network θ_{SN} with water content derived from cosmic-ray neutron sensing (CRNS) θ_{CRNS}, as applied within this study for the root mean square error (RMSE). Option 1 is the baseline comparison using the arithmetic mean from the sensor network $\theta_{SN(avg)}$ to compare with θ_{CRNS}, resulting in a baseline performance ($RMSE_{base}$). Option 2 is the bias comparison assessing the systematic deviation introduced by the additional hydrogen pools (AHP) that are subtracted from θ_{CRNS} resulting in a volumetric CRNS-derived soil moisture $\theta_{CRNS(vol)}$ that is compared with $\theta_{SN(avg)}$ in a bias performance ($RMSE_{bias}$). Option 3 is the standard procedure, where AHP are added to θ_{SN} and the sensor network is weighted $\theta_{SN(wt)}$ to better represent the water content sensed by CRNS. Comparison results in a reference performance ($RMSE_{ref}$) expected to be low compared with Option 1. Option 4 is showing the analysis conducted within this study, where CRNS-derived soil moisture is "unweighted" with a profile shape correction factor f_{pc}, AHP are removed, and profile shape corrected CRNS-derived soil moisture $\theta_{CRNS(pc)}$ is compared with $\theta_{SN(avg)}$ resulting in the profile shape correction performance ($RMSE_{pc}$). This approach is tested for different numbers of locations, radial distances, and depths of the locations present in the sensor networks

2.3 | Profile shape correction procedure

Baroni et al. (2018) proposed a simple profile shape correction to apply to CRNS-derived soil moisture. It accounts for the sensitivity of the sensor to the depth-dependent distribution of soil moisture within the profile. The shape of the soil moisture profile can be estimated only with additional information (e.g., observations or hydrologic modeling; Baatz et al., 2017; Han et al., 2016; Iwema, Rosolem, Rahman, Blyth, & Wagener, 2017; Rosolem et al., 2014). For the use of CRNS as a soil moisture monitoring method, this could be more practically achieved by few additional soil moisture measurements to determine the profile shape.

The procedure of the profile shape correction includes the following steps. A profile shape correction factor (f_{pc}) is calculated based on the simple arithmetic mean of a soil moisture profile [$\theta_{p(avg)}$] and the vertically weighted soil moisture profile [$\theta_{p(vwt)}$, Equation 6]. The CRNS-derived soil moisture (total weighted water content) is corrected ("unweighted") with this factor and in a final step AHP (i.e., lattice water and soil organic carbon water equivalent) are subtracted:

$$f_{pc} = \frac{\theta_{p(avg)}}{\theta_{p(vwt)}} \tag{8a}$$

$$\theta_{CRNS(non-wt)} = f_{pc} \cdot \theta_{CRNS} \tag{8b}$$

$$\theta_{CRNS(pc)} = \theta_{CRNS(non-wt)} - AHP \tag{8c}$$

The CRNS-derived soil moisture delivers and integral soil moisture value for its support volume; however, θ_{CRNS} represents a total weighted water content. Compared with the weighting procedure of point measurements (Section 2.2), the profile shape correction follows the reverse order. First, the soil moisture product is "unweighted," and second, the AHP are subtracted (compare also Figure 1). With this, the resulting $\theta_{CRNS(pc)}$ represents an easier to interpret integral soil moisture over the CRNS support volume.

2.4 | Assessment of CRNS-derived soil moisture and of the profile shape correction

To evaluate the difference between the soil moisture products from the sensor network and the CRNS and to evaluate the performance of the profile shape correction, different performance measures can be used. A well-established standard approach is the root mean square error (RMSE). It is a measure of the difference between two data series that can be prone to a biased dataset and outliers. A systematic bias can be shown by the more simple mean absolute error (MAE) that is the average absolute difference between the datasets (Chai & Draxler, 2014). Other performance measures in hydrology focus more on the ability of a model to simulate the observed time series dynamics—for example, the Nash–Sutcliffe efficiency (NSE) (ranging from $-\infty$ to 1, with 1 being the perfect match), and the Kling–Gupta efficiency (KGE) with the same range, including statistics of linear correlation, variability, and bias (Knoben, Freer, & Woods, 2019). To allow comparison of the results presented in this study with those of other literature, we use the common RMSE for the main analysis and also discuss results using the KGE (results for all performance measures and a detailed analysis for one field site are presented in Appendix D).

Soil moisture from the sensor networks and CRNS-derived soil moisture are compared for different processing steps. Figure 1 gives a graphical overview of the different comparisons and steps involved in the calculation (RMSE is listed as an exemplary measure). For a baseline comparison, the CRNS-derived soil moisture (θ_{CRNS}) is compared with the simple arithmetic mean of the distributed sensor network [$\theta_{SN(avg)}$] leading to a $RMSE_{base}$. Since CRNS-derived soil moisture represents a total weighted water content including additional hydrogen pools (AHP), deviations are expected to be high (Figure 1, Option 1). The systematic deviation introduced by the AHP can be assessed by subtracting them from θ_{CRNS} [resulting in $\theta_{CRNS(vol)}$] and comparing with $\theta_{SN(avg)}$, resulting in $RMSE_{bias}$. We call this comparison bias performance (Figure 1, Option 2). When AHP are added to the distributed sensor network and it is weighted after Schrön et al. (2017), $\theta_{SN(wt)}$ mimics the CRNS behavior. We use this as a reference performance and expect the lowest achievable deviations given by $RMSE_{ref}$ (Figure 1, Option 3). Applying the profile shape correction (i.e., unweighting and the removal of the AHP) on CRNS-derived soil moisture [$\theta_{CRNS(pc)}$] and comparing it with the sensor network $\theta_{SN(avg)}$ results in a profile shape correction performance measure, called $RMSE_{pc}$ (Figure 1, Option 4).

The $\theta_{CRNS(pc)}$ is obtained in three different ways: (a) using all soil moisture profile measurement locations and measurement depths; (b) using a reduced number of soil moisture profile measurement locations, based on distance to the CRNS; and (c) using the first and second approach with an incrementally reduced maximal measurement depth of the profile locations.

The analysis is repeated for all possible combinations of soil moisture measurement locations, based on the availability at each experimental site. Namely, a sensor network consists of n locations of profile measurements θ_p. This is sampled for different numbers of locations (sample size k), resulting in different amounts of possible combinations of locations. For example, a sensor network of $n = 16$ locations and a sample size of $k = 3$ profile locations results in 560 possible combinations. All cases are calculated when possible combinations are <800. A random sample of 800 cases are calculated when possible combinations >800. For larger samples, no change in results could be observed. This procedure is applied for all locations and depths of the sensor network.

The depth analysis is applied by reducing the depth stepwise to a minimum of the two shallowest measurements (to still be able to do a weighting), and the spatial analysis is applied by decreasing the number of considered locations n with the radial distance around the CRNS. The selected profile locations k of within a certain radius around the CRNS sensor r, down to the considered depth d, are then averaged for each depth to present an average field profile $\theta_{p(k,r,d)}$, which is used to calculate the profile shape correction factor f_{pc}.

2.5 | Field sites

The analyses are performed based on data collected at four experimental sites previously published. All four field sites used in this study were equipped with a CRNS and a distributed sensor network, and only periods when both measurements are available were considered in the analysis. The following paragraphs give a brief description of the field sites and previous work. Table 1 gives an overview of the main features and differences between the field sites, and Figure 2 outlines the different setups of their point sensor networks. The raw CRNS neutron counts for all sites were corrected for variations in air pressure, incoming radiation, and humidity; details on the procedure and the methods for the determination of additional hydrogen pools AHP and calibration are described in the original publications. Presented in this study is a 12-h moving average of CRNS-derived soil moisture to reduce statistical noise.

The dataset of Katharinentaler Hof (KAT) was used in a previous study by Baroni et al. (2018) to estimate the uncertainty and sensitivity of different parameters on the CRNS product. Based on their results, the profile shape correction tested in this study was proposed. The field site is located in southern Germany, close to Pforzheim (48.9285° N, 8.7028° E), at an elevation of 319 m asl. The soils are classified as silt loam (USDA soil texture classification), with soil textures in upper soil layers consisting of 3.4, 81.1, and 15.4%

TABLE 1 Main features of the four field sites showing measurement period, land use during the experiment, soil bulk density (ρ_b) and additional hydrogen pools (AHP), and the soil moisture regimes expressed as median and range from the respective sensor network [$\theta_{SN(avg)}$]

Field site[a]	Original publication	Measurement period	Mean annual precipitation	Annual mean temperature	Land use	ρ_b	AHP	$\theta_{SN(avg)}$ median (min.–max.)
			mm	˚C		g cm^{-3}	———	cm^3 cm^{-3} ———
KAT	Baroni et al. (2018)	4 Apr. 2013–31 July 2013	780	9.5	Winter wheat	1.48	0.015	0.34 (0.20–0.41)
HOAL	Franz et al. (2016)	12 Dec. 2013–26 Aug. 2014	823	9.5	Agriculture, diverse crops	1.38	0.061	0.34 (0.18–0.40)
SEL	Jakobi et al. (2018)	14 May 2016–24 Oct. 2016	714	10.2	Sugar beet	1.35	0.050	0.16 (0.10–0.33)
SRER	Franz, Zreda, Rosolem, & Ferre (2012b)	1 July 2011–31 July 2013	364	20.0	Creosote bush	1.41	0.018	0.04 (0.02–0.12)

[a]KAT, Katharinentaler Hof; HOAL, Hydrological Open Air Laboratory; SEL, Selhausen; SRER, Santa Rita Experimental Range.

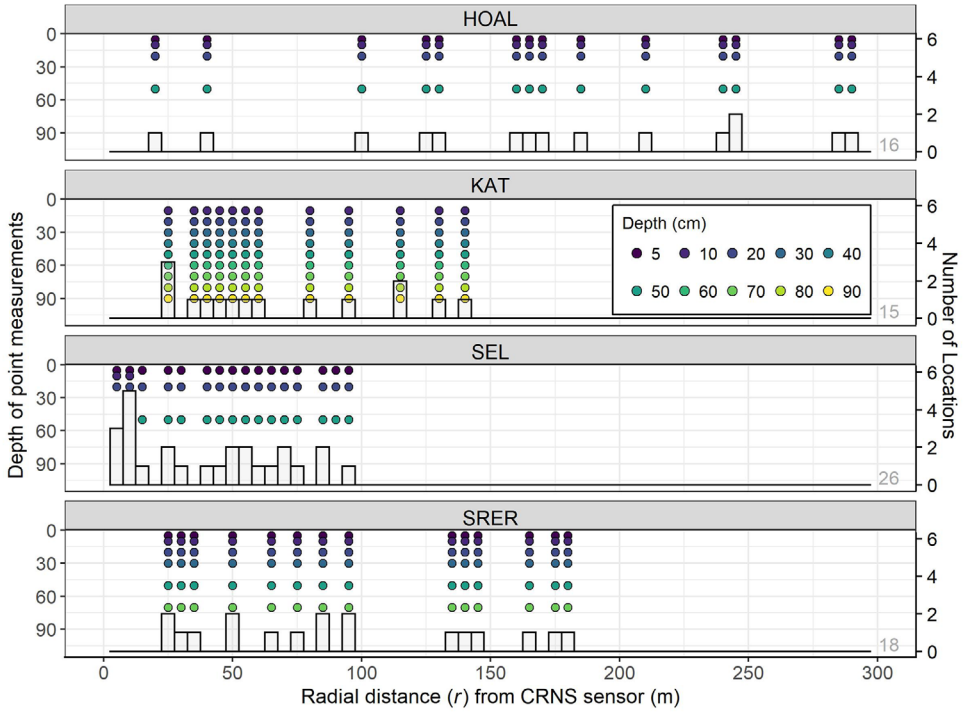

FIGURE 2 Setup of the distributed sensor network at the four field sites. Bars show the number of locations (right axis) at the specific radial distance (*x* axis) from the cosmic-ray neutron sensor (CRNS) in 5-m increments, and the colored dots show the depths of measurements (left axis) at these locations. Gray numbers in the bottom right of the panels show total number of locations within the sensor networks. HOAL, Hydrological Open Air Laboratory; KAT, Katharinentaler Hof; SEL, Selhausen; SRER, Santa Rita Experimental Range

of sand, silt, and clay, respectively (Imukova, Ingwersen, Hevart, & Streck, 2016). The 14-ha field was cropped with winter wheat (*Triticum aestivum* L.) during the study period. Plant height measurements were available on a weekly basis. The soil moisture monitoring network consists of 15 randomly distributed locations with profiles from 10-cm down to 90-cm depth at depth increments of 10 cm (Figure 2). A standard weather station recorded pressure, temperature, humidity and precipitation on the field. For details on the dataset, refer to Imukova et al. (2016) and Baroni et al. (2018).

The dataset of the Hydrological Open Air Laboratory in Petzenkirchen (HOAL) was used by Franz et al. (2016), who studied the performance of CRNS as representative of landscape average in a heterogeneous agricultural landscape; data

are available from the COsmic-ray Soil Moisture Observing System (COSMOS) website (http://cosmos.hwr.arizona.edu/). It is an agricultural field site in northeast Austria close to Petzenkirchen (48.1547° N, 15.1483 °E) at an elevation of 277 m asl. The soils are mainly silt loam with average textures of 8.4% sand, 71.3% silt, and 20.3% clay (Picciafuoco et al., 2019). The field footprint of the CRNS at HOAL covers diverse land use parcels with individual soil cultivation and main crops being winter wheat, barley (*Hordeum vulgare* L.), maize, and rape (*Brassica napus* L.) (for details refer to Table 1 in Franz et al., 2016). The influence of the vegetation on the CRNS signal is assumed to be small, as the landscape average fresh standing biomass is expected to be low (<2 kg m^{-2}; Franz et al., 2016). The distributed sensor network consists of 16 locations within the CRNS footprint; however, most locations are far from the sensor (>100 m), with sensors installed at depths of 5, 10, 20, and 50 cm (Figure 2). Due to agricultural management, several of the sensors had to be removed during the study period. A weather station on the field recorded pressure, temperature, relative humidity, and precipitation. Weather data were updated and are now completely available, in contrast with the data presented in Franz et al. (2016). This improved the humidity correction, and therefore slight differences in the presented CRNS-derived soil moistures can be observed (compare also with Franz et al., 2020).We should also note the longer time series used in the present study. During the vegetation season, greater heterogeneity within the footprint is expected, leading to overall higher RMSE values between soil moisture from CRNS and sensor network than those reported by Franz et al. (2016).

The data set of Selhausen (SEL) was used in the study of Jakobi et al. (2018) to investigate the influence of biomass on the CRNS signal and evaluate the usage of the ratio of bare and moderated neutron detectors to quantify the biomass and correct the CRNS signal accordingly. This field site is part of the TERrestrial Environmental Observatories (TERENO) network (Bogena et al., 2018). It is located in western Germany about 40 km west of Cologne (50.8666° N, 6.4561° E) at an elevation of 105 m asl. The soil is silt loam with 8–15% gravel and a particle size distribution of 12–18% sand, 52–63% silt, and 13–17% clay (Rudolph et al., 2015). In this study, five CRNS probes were pooled in the center of a 2.77-ha large agricultural field, and hourly neutron counts of all sensors were summed up. The field was cropped with sugar beet (*Beta vulgaris* L.) during the study period, and biomass measurements were taken on a monthly basis. A linear relationship was assumed to derive plant height from biomass water equivalent (Jakobi et al., 2018). Pressure, temperature, and relative humidity were recorded at the field site. The distributed sensor network is a SoilNet wireless sensor network (Bogena et al., 2010). Eighteen locations were distributed within the field to cover the heterogeneity of electromagnetic conductivity and thus water-holding capacity of the field and were equipped with sensors at 5-, 20-, and 50-cm depth. Three additional locations within 3-m distance and five additional locations within 11-m distance with sensors at 5-, 10-, and 20-cm depth were installed, based on the assumption that the CRNS is more sensitive to hydrogen sources at shorter distances (Figure 2).

The research site Santa Rita Experimental Range (SRER) is part of the COSMOS network (Zreda et al., 2012) and was published in several research papers already. One of the first studies was by Franz, Zreda, Rosolem, & Ferre (2012), who compared the CRNS to an accompanying distributed sensor network and tested the understanding of the effective sensor depth (Franz, Zreda, Ferre, et al., 2012). It is located ∼35 km south of Tucson, AZ (31.9085° N, 110.8394° W) at an elevation of 989 m asl. The vegetation at the site is sparse (∼24% cover) with low biomass (<2.5 kg m^{-2}; Huang, Marsh, McClaran, & Archer, 2007), mainly consisting of creosote bush [*Larrea tridentata* (DC.) Coville] and to a lesser extent of grasses, forbid, cacti, and mesquite. Biomass is also constant and is assumed to have a minor effect at this field site. The soil is sandy loam, with 5–15% gravel in the top meter and average particle size distribution of 72.5% sand, 13.0% silt, and 5.2% clay (Franz, Zreda, Rosolem, & Ferre, 2012; Schreiner-McGraw et al., 2016). Weather data were collected onsite, associated with an eddy covariance station, and several rain buckets were distributed in the catchment. The distributed sensor network consists of 18 locations within the footprint of the CRNS, with sensors installed at 10-, 20-, 30-, 50-, and 70-cm depth and from January 2012; data from sensors at 5-cm depth are also available (Figure 2). At each location, there were paired sensors beneath the canopy and in the intercanopy space, which were treated as one location within this study.

3 | RESULTS AND DISCUSSION

3.1 | Application of the profile shape correction

The CRNS and the sensor network were compared using the different options as described in Section 2.4 and summarized in Figure 1 for baseline performance, bias performance, reference performance, and the profile shape correction. Table 2 lists the resulting performance measures RMSE and KGE for all field sites. The profile shape correction was based on all data available from the sensor networks (i.e., soil moisture values at all the radial distances and depths and at all available locations). For SEL, the closest eight locations were excluded, as the sensors were not installed down to the maximum depth (Figure 2).

The $RMSE_{base}$ of HOAL and SEL are high, KAT shows an intermediate value, and SRER has the lowest $RMSE_{base}$, which is also a consequence of the generally low soil moisture at this site (Table 1). For all field sites, the

TABLE 2 The performance measures RMSE ($m^3\ m^{-3}$) and Kling–Gupta efficiency (KGE) for the four different field sites. For the baseline comparison (base), the averaged sensor network is compared with cosmic-ray neutron sensing (CRNS)-derived soil moisture. With the bias performance (bias), the effect of dealing only with additional hydrogen pools (AHP) is assessed by subtracting them from CRNS-derived soil moisture and comparing with the averaged sensor network. For the reference performance (ref), the weighted sensor network including AHP is compared with CRNS-derived soil moisture; this is assumed to lead to best possible comparability between the datasets. To measure the performance of the profile shape correction (pc), the averaged sensor network and the profile-shape-corrected, CRNS-derived soil moisture are compared. The vertical weighting follows the Köhli approach (D_K)

Field site[a]	Measure	base	bias	ref	pc[b]
KAT	RMSE	0.047	0.038	0.032	0.031
	KGE	0.59	0.60	0.86	0.80
HOAL	RMSE	0.064	0.059	0.054	0.059
	KGE	0.44	0.45	0.54	0.23
SEL	RMSE	0.066	0.046	0.046	0.041
	KGE	0.58	0.66	0.70	0.70
SRER	RMSE	0.037	0.026	0.019	0.016
	KGE	−0.17	-0.03	0.68	0.60

[a]KAT, Katharinentaler Hof; HOAL, Hydrological Open Air Laboratory; SEL, Selhausen; SRER, Santa Rita Experimental Range.

[b]Profile shape correction is based on different measurement depths, radial distances, and sample sizes (d, r, and k) for the field sites: KAT (90, 150, and 15), HOAL (50, 320, and 16), SEL (50, 100, and 18), and SRER (70, 200, and 18).

weighting of the sensor network leads to better comparability ($RMSE_{ref} < RMSE_{base}$). However, the level of improvement varies between field sites. For KAT, the $RMSE_{ref}$ is well in range with other studies of similar setups (Coopersmith et al., 2014; Tian, Li, Liu, Li, & Ren, 2016), and an improvement of 0.016 $m^3\ m^{-3}$ compared with $RMSE_{base}$ is achieved. Similarly, for SEL, considering AHP and the weighting improves the comparison by 0.020 $m^3\ m^{-3}$, and the $RMSE_{ref}$ is still within an acceptable range as compared with results from other studies for humid environments and low elevation (Rivera Villarreyes et al., 2011). The SRER site shows an already low $RMSE_{base}$ value, and RMSE is further reduced by 0.018 $m^3\ m^{-3}$ when weighting the sensor network in the reference performance. Within previous studies, the accuracy of CRNS at this field site was already shown to be high (Franz, Zreda, Ferre, et al., 2012; Franz, Zreda, Rosolem, & Ferre, 2012). At HOAL, the $RMSE_{ref}$ shows an improvement of 0.010 $m^3\ m^{-3}$ compared with the $RMSE_{base}$ value. The low RMSE value as reported in Franz et al. (2016) could not be reproduced within this study, because the CRNS data are based on different weather data for the humidity correction, and a longer time series with higher heterogeneity of in situ soil moisture during the vegetation season is used here. For all field sites, the profile shape correction leads to $RMSE_{pc}$ values lower than the $RMSE_{base}$ when using all the information available from the distributed sensor network. The values are even lower than the $RMSE_{ref}$, except for HOAL. The performance at this field site can be explained by point soil moisture measurements being located farther from the CRNS probe, which will be shown within the sections below. The proposed profile shape correction can thus be assumed to lead to equally good results as the weighting of the distributed sensor network. The systematic deviation introduced by AHP, as assessed by $RMSE_{bias}$, explains about half of the improvement between $RMSE_{base}$ and $RMSE_{ref}$ for the field sites of KAT, HOAL, and SRER. At these field sites, the consideration of AHP is as important as considering the weighting. For SEL, the subtraction of AHP explains a larger share of the improvement in the performance measures.

Results for KGE in Table 2 show a similar trend as the RMSE values. In all cases, better performance is reached with higher KGE_{ref} compared with KGE_{base}, with the clearest improvement (0.85) for SRER. The consideration of the bias from AHP does not lead to a large improvement compared with the baseline performance (≤0.01) in the case of KAT and HOAL., For SEL and SRER, the improvement in KGE_{bias} is 0.08 and 0.14, respectively. For SEL, KGE_{pc} does reach reference performance, whereas for the other field sites, KGE_{pc} remains lower than KGE_{ref}. This is especially true for HOAL, the only field site with lower KGE_{pc} than KGE_{bias}. Similar to the performance of $RMSE_{pc}$ at HOAL, this is attributed to point soil moisture measurements being located farther from the CRNS probe. Although the weighting of the sensor network includes a horizontal weighting (represented by low values in KGE_{ref}), the profile shape correction is based on a vertical weighting only and is thus stronger affected by less representative soil moisture profiles of distant locations and results improve when only closer locations are used. For the profile shape correction at HOAL, $d \leq 50$ cm, $r \leq 100$ m, and $k = 3$ results in KGE_{pc} of 0.046. This is in agreement with the performance improvement for the other field sites. The KGE emphasizes the match of the soil moisture dynamics between the two time series. The weighting introduces a dynamic on sensor network data [$\theta_{SN(wt)}$] closely matching the higher variability observed in CRNS-derived soil moisture time series θ_{CRNS} (high KGE values for the reference performance). In contrast, the profile shape correction is based on the ratio of the simple average and the weighted soil moisture profile, and higher variability remains within $\theta_{CRNS(pc)}$ compared with variability in $\theta_{SN(avg)}$. Consequently, the KGE_{pc} does not reach the reference performance. Considering the weighting is more important for the improvement of KGE for three of the four field sites (KAT, HOAL, and SRER) than addressing the systematic deviation from AHP. The following results are discussed considering only the RMSE as a performance measure. However, the results found using the RMSE also apply for the other considered performance

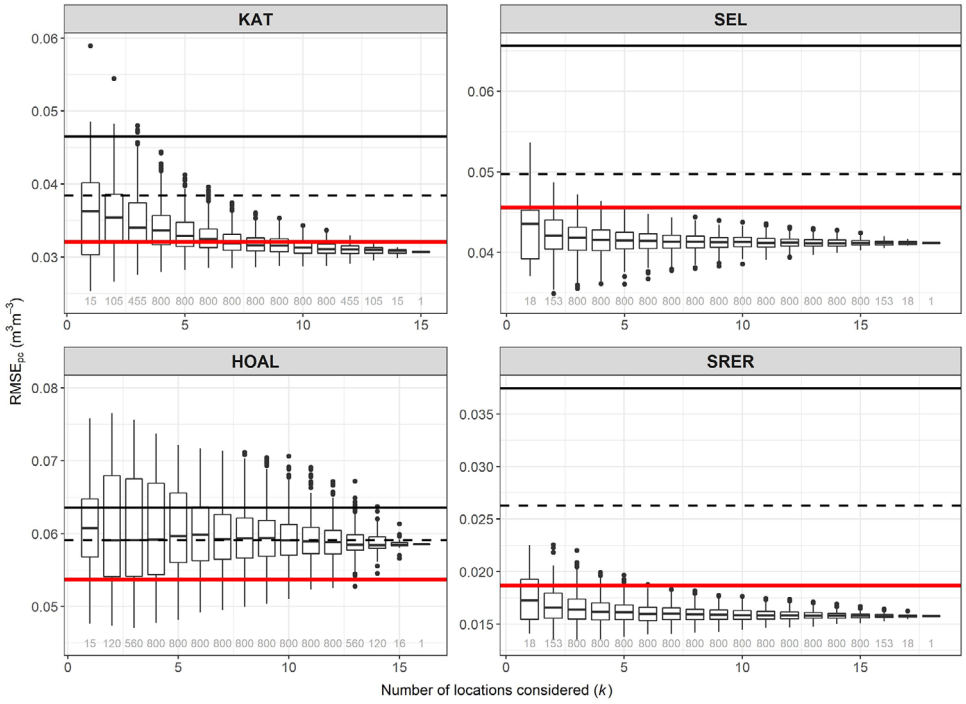

FIGURE 3 Results of the analysis conducted within this study, performance is assessed using the root mean square error (RMSE). For the maximum radial distance (r) and maximum depth (d), the number of locations to apply the profile shape correction (x axis, k) is changed. This results in $RMSE_{pc}$ (profile shape correction performance) values (y axis) for all possible location combinations (numbers given in gray below the box plots, a maximum of 800 combinations was set). The black line marks the $RMSE_{base}$ (baseline performance), the dashed the $RMSE_{bias}$ (bias performance), and the red line the $RMSE_{ref}$ (reference performance). HOAL, Hydrological Open Air Laboratory; KAT, Katharinentaler Hof; SEL, Selhausen; SRER, Santa Rita Experimental Range

measures (see Appendix D with a table also showing MAE and NSE for all field sites and a more detailed analysis with all four performance measures for the field site KAT).

Figure 3 gives an overview of $RMSE_{pc}$ for varying the number of soil moisture profiles k used to calculate the profile shape correction. The box plots shown in the graph consist of different numbers of samples due to combinatorics; the actual number of samples is given in numbers below the boxes. It is shown that the use of more locations to derive the field mean soil moisture profile $\theta_{p(k,r,d)}$ decreases the median of the $RMSE_{pc}$ and the range of the results. The $RMSE_{pc}$ for using all available locations at the field sites for maximum radial distance and depth is the same as presented in Table 2. Similar results were found by Brocca, Melone, Moramarco, and Morbidelli (2010) when comparing time series of randomly sampled locations to the mean of a sensor network.

3.2 | Influence of the measurement depth of the sensor network

We analyzed the depth to which information of a distributed sensor network is needed to deliver good results. For HOAL and SEL, only measurements down to 50 cm were available, whereas for SRER and KAT, point measurements extend down to 70 and 90 cm, respectively (Figure 2). For all field sites, the depth of the point measurements was reduced to the two shallowest depths for applying the profile shape correction, and deeper measurements were added subsequently for the analysis. Reduced measurement depth influences the estimation of the penetration depth and the calculation of vertical weights.

Figure 4 shows the results of considering different maximal measurement depths for the profile shape correction for all field sites. All available locations of the sensor networks were used to achieve most stable results (Section 3.1).

The $RMSE_{pc}$ values decrease using depths down to 50 cm for KAT, SEL, and SRER. For SEL and HOAL, only measurements down to 50-cm depth are available, and for SEL, different measurement depth were available at different locations. Considering depths down to 50 or 60 cm leads to best $RMSE_{pc}$ values for KAT, and values increase with more shallow or deeper depths. For SRER a slight improvement can be observed using depth down to 70 cm, which can be attributed to the generally higher penetration depth of the CRNS at the field site due to low soil moisture values. At SEL also, using a depth down to 50 cm leads to better results, even though only the locations farther away are equipped with sensors to this depth. Comparable results were found by Ragab et al. (2017), where CRNS was shown to be representative for soil moisture

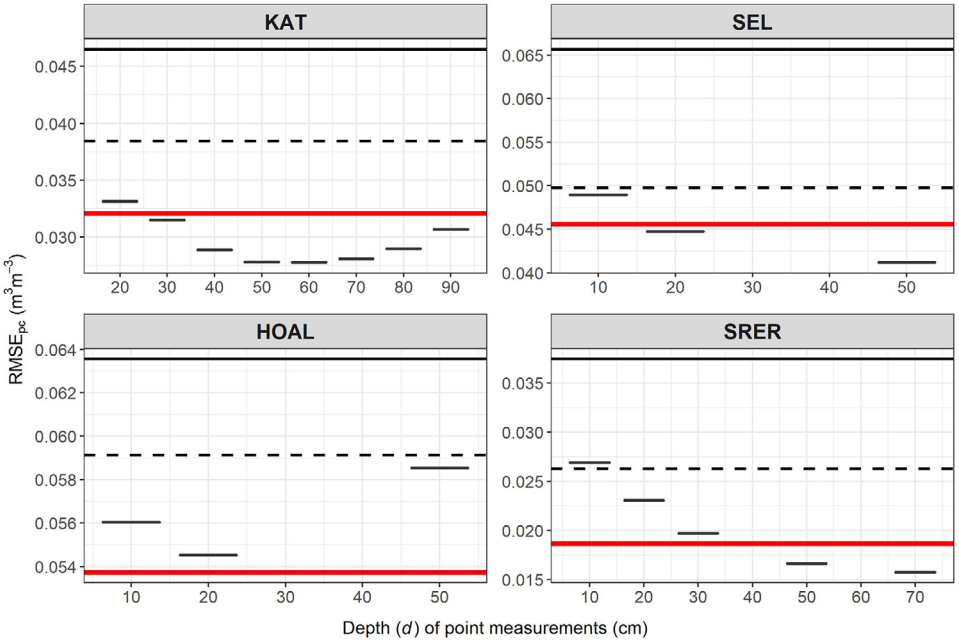

FIGURE 4 RMSE$_{pc}$ (profile shape correction performance using the root mean square error [RMSE]) for considering different depth for the profile shape correction using all available locations of the sensor networks. The red line marks the RMSE$_{ref}$ (reference performance), the black line marks the RMSE$_{base}$ (baseline performance), and the dashed line marks the RMSE$_{bias}$ (bias performance). Note for SEL that not all depths were available at each of the measurement locations (10-cm depth only available for the closest locations, Figure 2). HOAL, Hydrological Open Air Laboratory; KAT, Katharinentaler Hof; SEL, Selhausen; SRER, Santa Rita Experimental Range

averaged over a depth of 10–60 cm, which was different from the shallower theoretical effective penetration depth.

At HOAL, however, lower RMSE$_{pc}$ values could be achieved when using only measurements down to 20 cm, compared with using measurements down to 50 cm. At this field site, the question of which measurement depth leads to good results cannot be separated from the question of which radial distance we use to achieve good results from the profile shape correction, which is discussed in the section below.

3.3 | Influence of the radial distance of point locations to the CRNS

To analyze the effect of the radial distance on the resulting RMSE$_{pc}$, an analysis was conducted considering only locations within a certain radius. The radius and thus the number of point locations was subsequently increased. Figure 5 shows the results for all field sites using all available locations for the profile shape correction (gray numbers below bars) and measurement depth of 50 cm. At SEL, only the 18 locations with depth down to 50 cm are included in the analysis.

For KAT, SEL, and SRER, RMSE$_{pc}$ values are below RMSE$_{ref}$ for all distances. The radial distances of sensor network locations at these field sites approximately equals the minimum horizontal footprint radius at these field sites (110 m for KAT and SEL, 180 m for SRER). Only at HOAL locations are also located at greater distances than the minimum horizontal footprint radius (120 m). For HOAL, using only locations within a radius of 150 m leads to RMSE$_{pc}$ values below the RMSE$_{ref}$. Using point information of locations with a larger radial distance increases the RMSE$_{pc}$ values. This is also the reason for the higher RMSE$_{pc}$ value compared with RMSE$_{ref}$, as presented in Table 2, where all point locations of the sensor network were used for the profile shape correction. The better performance of the 20-cm measurement depth in the section above is explained by considering that the penetration depth of the CRNS sensor decreases with increasing distance from the sensor. Thus, using measurement depths down to 20 cm improves the result for locations farther away, because shallow measurements are more representative of the areal average sensed by CRNS (Köhli et al., 2015; Schrön et al., 2017).

At SEL, improved results from locations within a close range to the CRNS sensor were expected, because of the sensitivity response of the sensor (Köhli et al., 2015). However, these locations only had reference measurements down to 20-cm depth, and the RMSE$_{pc}$ for using all locations within a radius of 11 m from the sensor is 0.047 m^3 m^{-3} (higher than the RMSE$_{ref}$), showing the importance of the measurement depth to be representative of the effective penetration depth.

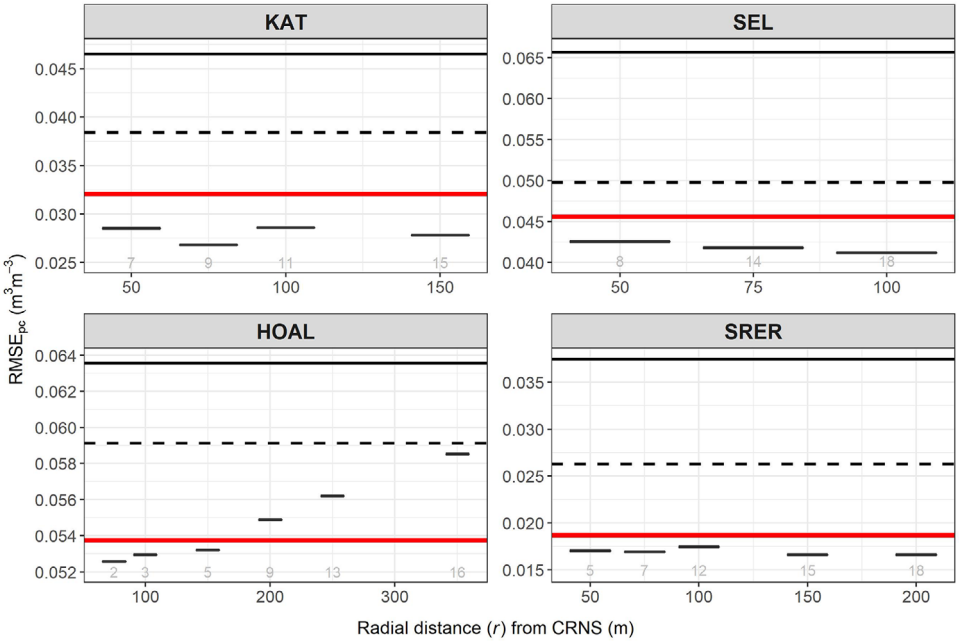

FIGURE 5 RMSE$_{pc}$ (profile shape correction performance using the root mean square error [RMSE]) considering different radial distances of the point soil moisture locations from the cosmic-ray neutron sensor (CRNS). With increasing radii, the number of available locations used for the profile shape correction increases (gray numbers below boxes). The red line marks the RMSE$_{ref}$ (reference performance), and the black line marks the RMSE$_{base}$ (baseline performance), and the dashed line marks the RMSE$_{bias}$ (bias performance). HOAL, Hydrological Open Air Laboratory; KAT, Katharinentaler Hof; SEL, Selhausen; SRER, Santa Rita Experimental Range

3.4 | Optimum number of point locations for profile shape correction

The sections above show the influence of the number of profiles, the measurement depth, and the distance of point locations on RMSE$_{pc}$. The best results can be achieved by using a measurement depth of at least 50 cm and using locations within the minimum effective radius. When more locations are considered, more stable and lower RMSE$_{pc}$ values are obtained. However, the goal for pragmatic monitoring is to be as parsimonious as possible with the additional profile measurements accompanying a CRNS. Figure 6 shows the results of using up to three point locations (k) for the profile shape correction for a radial distance $r \leq 75$ m (only HOAL $r \leq 100$ m, to get a sufficient number of locations at all) and a depth $d \leq 50$ cm for all field sites.

The results show that one location used for the profile shape correction already leads to improvement and RMSE$_{pc}$ values below the RMSE$_{base}$, except for HOAL with a median even below the RMSE$_{bias}$. The median decreases from RMSE$_{base}$ to RMSE$_{pc}$ by 0.018 (38%), 0.022 (33%), 0.007 (11%), and 0.019 (53%) at the field sites KAT, SEL, HOAL, and SRER, respectively. Using three locations to derive the field mean soil moisture profile and apply the profile shape correction leads to median RMSE$_{pc}$ values below the RMSE$_{ref}$ for all field sites.

Brocca et al. (2010) also found a maximum of four locations of their sensor network cluster to lead to sufficiently low RMSE to validate remote-sensing products. At the field scale, the same number of locations was found to correctly represent the average temporal variability of the soil moisture with high accuracy.

In some cases, the profile shape correction gives even better results than the weighting of a complete sensor network. For a sensor network, many locations are necessary to obtain a representative absolute value of the spatial mean, and different wetness conditions can still lead to different patterns of soil moisture within the field (Baroni, Ortuani, Facchi, & Gandolfi, 2013). The weighting of the sensor network is based on the absolute soil moisture values, and the influence of less representative measurements might increase through the weighting procedure (Brocca et al., 2010; Nguyen et al., 2017). Cosmic-ray neutron sensing, on the other hand, always senses an integral value independent of the small-scale heterogeneity, even though changes in horizontal footprint and effective measurement depth are observed. Only a few measurement locations are representative of the field-scale soil moisture profile and wetting or drying states that influence the CRNS vertical sensing depth. The correction factor is solely based on the ratio of the weighted and nonweighted soil moisture profile. Because only the ratio is used, the influence of absolute soil moisture values is reduced, and generally

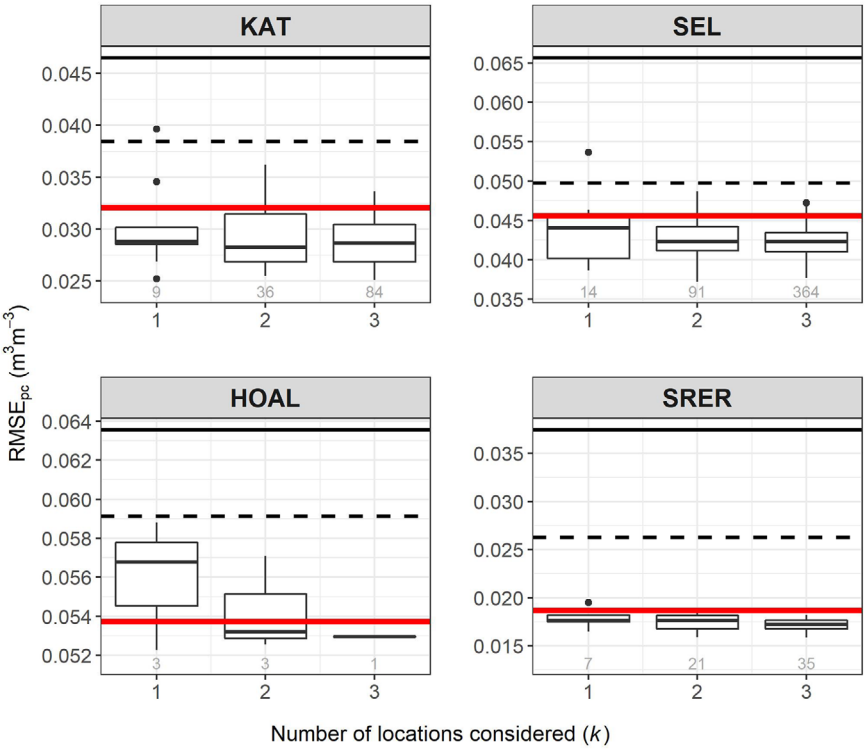

FIGURE 6 Results in $RMSE_{pc}$ (profile shape correction performance using the root mean square error [RMSE]) for using one to three locations (k) for the profile shape correction for all field sites (depth $d \leq 50$ cm, radial distance $r < 75$ m for Katharinentaler Hof [KAT], Santa Rita Experimental Range [SRER], and Selhausen [SEL] and $r \leq 100$ m for Hydrological Open Air Laboratory [HOAL]). The black line marks the $RMSE_{base}$ (baseline performance), the dashed line marks the $RMSE_{bias}$ (bias performance), and the red line marks the $RMSE_{ref}$ (reference performance). Numbers below the boxes show the amount of location combinations contained in the boxes

wetter or dryer locations sufficiently characterize the profile shape.

3.5 | Influence of the vertical weighting method

Within this study, it was also tested whether the choice of the vertical weighting method influences the results. The results presented above are based on D_K (Section 2.2).

Using D_F for the profile shape correction produces similar results. The general trend as shown in Figure 3 for the analysis of the profile shape correction is the same for both weighting methods—using more locations gives lower and more stable results (data not shown). Also, the use of a measurement depth of up to 50 cm and a radial distance of <75 m (100 m for HOAL), as well as the number of locations needed to achieve results as good as the $RMSE_{ref}$, is confirmed using D_F (data not shown). In Figure 7, the weighting options are compared using $k \leq 3$, $d \leq 50$ cm, and $r \leq 75$ m (for HAOL, $r \leq 100$ m). Median $RMSE_{pc}$ values differ by a maximum of 0.002 m^3 m^{-3} for the field sites KAT and SEL (Figure 7), with D_K performing better at KAT and D_F performing better at SEL. However, the range of $RMSE_{pc}$ tends to be greater when using the Franz weighting approach. For HOAL and SRER, the differences are even smaller.

For the calibration and weighting of a sensor network to compare water content with CRNS measurements, the Köhli nonlinear vertical and horizontal weighting approach outperforms the Franz approach in the studies of Schrön et al. (2017) and Cai et al. (2018), whereas Nguyen et al. (2017) found that a linear weighting leads to better results. Dimitrova-Petrova et al. (2020) could not find a difference using either of the vertical weighting options on the estimated near-surface water storage used in rainfall-runoff modeling. This was also confirmed for the vertical weighting in the study of Sigouin, Dyck, Si, and Hu (2016). Although this might also depend on site-specific characteristics, to define the general profile shape within the profile shape correction, linear and nonlinear vertical weighting options seem to be equally applicable. We also conclude that both vertical weighting options can be used for the profile shape correction.

3.6 | Example of applying the profile shape correction

Figure 8 shows the time series of soil moisture and the application of the profile shape correction for the field site KAT in relation to precipitation (Panel a). Panel b shows θ_{CRNS}, $\theta_{SN(avg)}$, and the standard weighting of the sensor network $\theta_{SN(wt)}$. Because of the sensitivity of CRNS to upper soil layers, precipitation events and resulting wetting fronts θ_{CRNS} show higher variability within the soil moisture time series compared with $\theta_{SN(avg)}$ (Franz, Zreda, Ferre, et al., 2012), and the systematic deviation of AHP contained in θ_{CRNS} leads to an offset between the two time series. The inclusion of AHP and the weighting in $\theta_{SN(wt)}$ accounts well

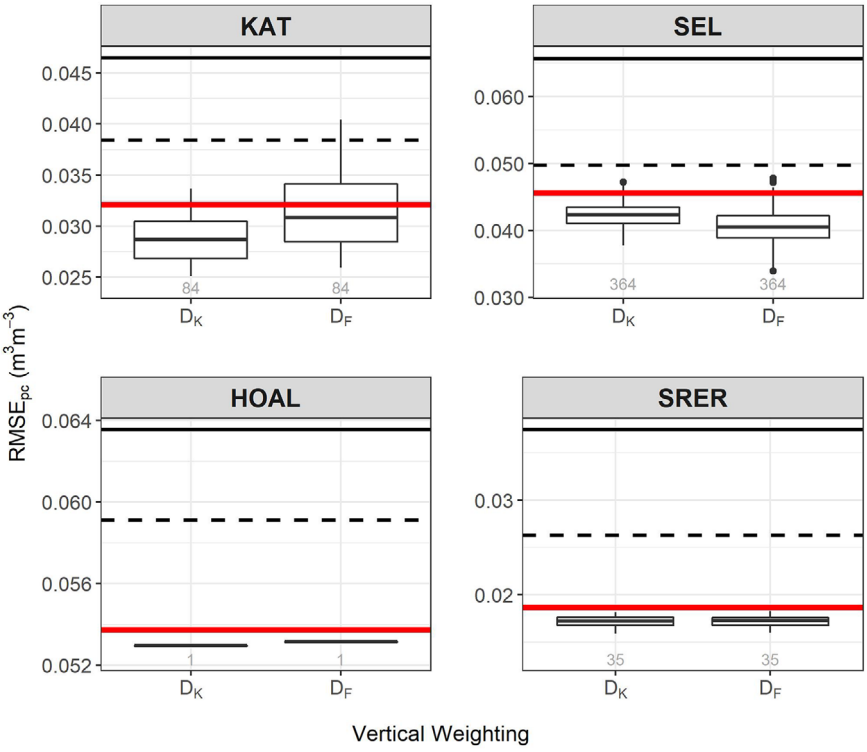

FIGURE 7 Results in $RMSE_{pc}$ (profile shape correction performance using the root mean square error [RMSE]) of using the different vertical weighting options D_K (following Köhli et al., 2015) and D_F (following Franz, Zreda, Ferre, et al., 2012) for all field sites. The correction is based on locations $k \leq 3$ profiles with depth $d \leq 50$ cm, radial distance $r \leq 75$ m (except for HOAL $r \leq 100$ m). The total number of possible combinations of locations is given in gray numbers below the boxes. The red line marks the $RMSE_{ref}$ (reference performance), the black line marks the $RMSE_{base}$ (baseline performance), and the dashed marks the $RMSE_{bias}$ (bias performance). HOAL, Hydrological Open Air Laboratory; KAT, Katharinentaler Hof; SEL, Selhausen; SRER, Santa Rita Experimental Range

for this, and differences from θ_{CRNS} and are small. Deviations between $\theta_{SN(wt)}$ and θ_{CRNS} in the second part of June can be observed as a consequence of precipitation events that are reflected in the CRNS water content but are not visible in the time series of the sensor network because of the loamy soils and the shallowest point sensor installed at 10-cm depth only. Also, during the drying period after the large precipitation event at the beginning of June, $\theta_{SN(wt)}$ and θ_{CRNS} deviate. We observed periods for other field sites where the weighting did not account well for CRNS in cases of a drying soil moisture profile (data not shown). Deviations between θ_{CRNS} and $\theta_{SN(avg)}$ are shaded in red in Panel b. For this example, the profile shape correction factor (Panel c) is based on the median of the results as presented in Figure 6 [field mean profile $\theta_{p(k,r,d)}$ with $k = 3$, $r \leq 75$ m, and $d \leq 50$ cm] to calculate $\theta_{CRNS(pc)}$ (Panel d). The $\theta_{CRNS(pc)}$ better matches the absolute values of $\theta_{SN(avg)}$ in comparison with θ_{CRNS}, and only for the driest time of the time series after middle of July, higher deviations occur (shaded in blue) and $\theta_{CRNS(pc)}$ underestimates $\theta_{SN(avg)}$ clearly. The $\theta_{CRNS(pc)}$ still shows a greater dynamic than observed in data from the sensor network. This is, to a minor degree, a consequence of statistical variability in the neutron signal but is also due to the high sensitivity of the CRNS to upper soil layers (Franz, Zreda, Ferre, & Rosolem, 2013; Lv, Franz, Robinson, & Jones, 2014), whereas the shallowest measurements of the sensor network are at 10-cm depth.

Deviations between $\theta_{SN(wt)}$ and θ_{CRNS} as well as the deviations between $\theta_{CRNS(pc)}$ and $\theta_{SN(avg)}$ are shown as time series in Panel e for better comparison. They are very similar until the middle of June, showing that the profile shape correction performs as well as the weighting of the sensor network. From the middle of June on, the deviations differ as a consequence of using three locations for the profile shape correction, compared with using all locations for weighting the soil moisture network. During this drying period, soil moisture sensors at these three locations have a drift compared with the field average soil moisture. The deviations are similar during the entire season, when the profile shape correction is based not on three, but all available locations (data not shown). The drift when using three locations, however, does not generally lead to worse results, the profile shape correction performs better until the second week of June (deviations closer to 0), and only afterwards the deviations of the profile shape correction are higher.

Time series of the other three field sites confirm the applicability of the profile shape correction (data not shown). As soon as $\theta_{SN(wt)}$ mimics the dynamics of θ_{CRNS} well, the correction also leads to $\theta_{CRNS(pc)}$ values close to $\theta_{SN(avg)}$. For SRER, for example, $\theta_{SN(wt)}$ follows θ_{CRNS} dynamics very well during precipitation events. During dry times however, the time series deviate clearly, and accordingly the profile shape correction and resulting $\theta_{CRNS(pc)}$ do not match $\theta_{SN(avg)}$. A similar case was found for another field site with heavy clay soils, influence of shallow groundwater, and thus a very strong soil moisture gradient within the profile during dry periods (0.2 m^3 m^{-3} at 5-cm depth to 0.5 m^3 m^{-3} at 20-cm depth, data not shown). For such periods, we observed

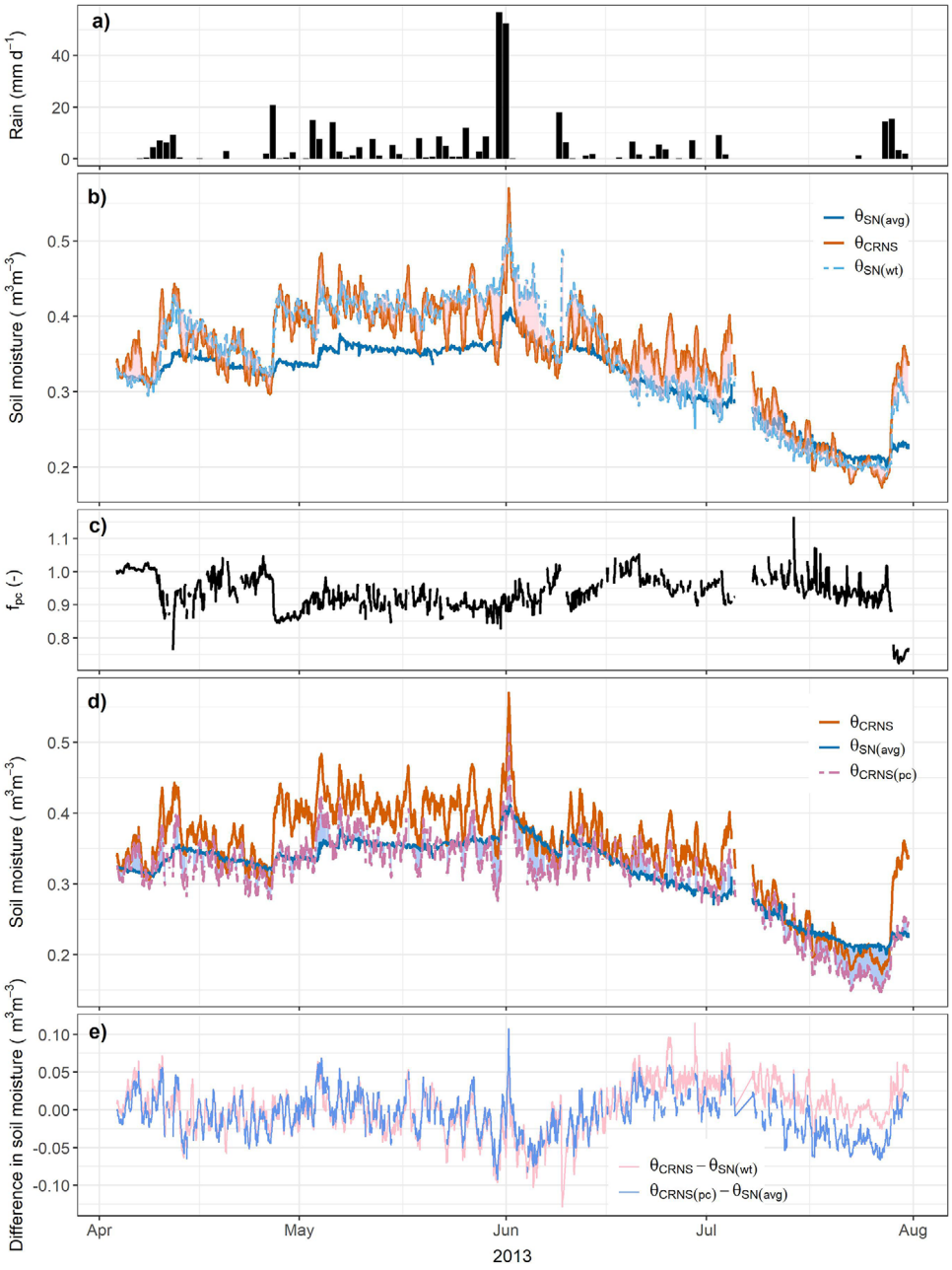

FIGURE 8 Example of the profile shape correction at the field site Katharinentaler Hof (KAT). Panel a shows the daily precipitation. Panel b shows the time series of soil moisture derived from cosmic-ray neutron sensing (θ_{CRNS}), the volumetric average soil moisture from the sensor network [$\theta_{SN(avg)}$], and the weighted soil moisture following the standard approach [$\theta_{SN(wt)}$]. Panel c shows the correction factor f_{pc} based on a field mean profile $\theta_{p(k,r,d)}$ with locations $k = 3$, radial distance $r \leq 75$ m, depth $d \leq 50$ cm. Panel d again shows θ_{CRNS} and $\theta_{SN(avg)}$ and the profile shape corrected cosmic-ray neutron sensing [$\theta_{CRNS(pc)}$]. Panel e shows the deviations between soil moisture time series as shown in shaded areas in Panels b and d

the weighting function and resulting $\theta_{SN(wt)}$ not being able to reproduce θ_{CRNS}. In contrast, Franz, Zreda, Ferre, et al. (2012) found lower deviations during evaporation and drainage periods than for infiltration fronts from simulation results. The systematic deviations we observe might be an issue of how to obtain the CRNS effective penetration depth for the weighting (d^* or D_{86}, depending on weighting option, see Section 2.2 and equations therein), which is calculated from the average water content of a profile. The average might not be sufficient to represent how deep the neutrons actually travel. A consideration of the depth-dependent distribution of soil moisture to derive the effective penetration depth of the sensor might be necessary. To assess the correct working of the weighting function was not the aim of this study, but this should be investigated in future research with the help of numerical analyses and similar modeling frameworks as

studied by Franz, Zreda, Ferre, et al. (2012), including soil moisture and neutron simulations.

There might be further reasons for deviations between CRNS and a sensor network. The latter detects only soil moisture, whereas CRNS potentially also detects biomass, interception, and ponding water (Baroni & Oswald, 2015). Also, a change in bulk density, as it might occur with changing wetness conditions or during a season within agricultural field sites or changes in organic carbon stocks, might influence the CRNS measurements (Avery et al., 2016; Wuest, 2014, 2015). Cosmic-ray neutron sensing is very sensitive to the shallow soil layers, where often no point sensors are installed (Lv et al., 2014), and the point sensors cover only specific installation depths, which can lead to a mismatch in vertical representativeness and differences between θ_{CRNS} and $\theta_{SN(wt)}$.

3.7 | Selection of the locations to measure the soil moisture profile

The analyses conducted showed that a profile shape correction based on one to three additional point soil moisture sensor profiles achieves good performance in addressing the vertical sensitivity of the CRNS signal. The analyses also showed that soil moisture profiles should be located relatively close to the probe where the CRNS signal is more sensitive to soil moisture dynamics. These conclusions are supported by the results obtained at four experimental sites that represent different soil hydrological conditions. For this reason, we recommend installing soil moisture sensor profiles along with a standard CRNS and applying the profile shape correction. The additional point locations, however, should be carefully positioned based on site characteristics and additional considerations. First of all, when recommending additional profile measurements, it is important to underline that the goal of these additional measurements is not to find the absolute soil moisture values or the time-stable locations that best represent the average soil moisture of the field site. Of course, having a single time-stable location to complement the CRNS measurements (as determined in Nguyen et al., 2017, 2019; Zhu et al., 2017) could be an advantage. However, this would require additional prior survey because it is not possible to determine such a location before the installation of the point sensors (Vanderlinden et al., 2012).

In contrast, the aim of the additional profile measurements is to characterize the shape of the soil moisture profile following infiltration fronts (e.g., by precipitation) and drying events (by atmospheric forcing or soil moisture redistribution) within the CRNS footprint. Since these are similar throughout a field site, even though some locations might be generally wetter or dryer than the average of the field (Hupet & Vanclooster, 2002), the selection of the location should be less critical.

We also addressed this issue with the data collected at the field site SEL, where a detailed map of geophysical properties (z-transformed electromagnetic conductivity distribution) is available (Rudolph et al., 2015). Therefore, we separated the sensor network locations into coarse grained areas ("dry") and areas with fine material fillings ("wet"). Results showed that, probing only "wet" or "dry" locations, $RMSE_{pc}$ differed by only 0.002 cm^3 cm^{-3} from results presented above (Table 2, Section 3.1) and thus can be neglected based on our results. Similar conclusions were obtained by a modeling study from Franz, Zreda, Ferre, and Rosolem (2013) and Baroni et al. (2018), where it was shown that CRNS signal was not sensitive to horizontal soil heterogeneity.

Significant differences might be found, however, when vegetation types or soil management (e.g., tillage and irrigation) lead to heterogenic profile shapes. For field sites with known and pronounced heterogeneities within the CRNS footprint, we suggest to cover those areas with the additional point measurements to derive a representative profile shape (Brocca et al., 2010; Sigouin et al., 2016). Another option could be to use soil hydrological models instead of measurements to predict the soil moisture profile shape. This would avoid the need of invasive measurements and would also have the advantage to be able to predict the shallow parts of the root zone, where CRNS is very sensitive but is often not monitored with point sensors (Lv et al., 2014). However, we also acknowledge that a model comes with uncertainties regarding input and parameters (Sigouin et al., 2016). Additionally, time and expertise are required for setting up and evaluating the model. For this reason, it might be easier to use complementary measurements as shown in this study, and we suggest further research on developing simple modeling approaches to predict the soil moisture profiles.

4 | SUMMARY AND CONCLUSIONS

Cosmic-ray neutron sensing-derived soil moisture within this study represents a total water content, including additional hydrogen pools (AHP) and an inherent weighting resulting from the sensitivity of the method. When comparing CRNS-derived soil moisture to the simple average retrieved from a soil moisture sensor network, great deviations occur (baseline performance), because of the inherent weighting and AHP contained in CRNS-derived soil moisture. To achieve high levels of accordance (reference performance), the CRNS-derived soil moisture is evaluated against a CRNS-specific weighted average from a soil moisture sensor network that accounts for this sensitivity and also includes AHP. The systematic deviation of AHP is assessed with AHP subtracted from CRNS-derived soil moisture and a comparison with the simple average of the sensor network (bias performance). On

the contrary, the weighting effect so far could only be considered when a forward operator (Shuttleworth et al., 2013) is coupled to a soil–hydrological model providing considerable limitations on the direct use of CRNS-derived soil moisture.

Within this study, a new and simple profile shape correction (Baroni et al., 2018) to account for the vertical sensitivity of CRNS-derived soil moisture by correcting for the depth-dependent distribution of soil moisture within the profile was systematically tested based on four datasets of CRNS-derived soil moisture and an accompanying distributed sensor network. The sensor network was randomly sampled for different numbers of locations and different distances and depths. Different vertical weighting options were also considered.

The results show that the profile shape correction on CRNS-derived soil moisture leads to a similar "reference performance" when compared with the averaged sensor network. Thus, the correction effectively reduces the influence of the CRNS vertical sensitivity and resulting soil moisture time series. The performance and stability of the results decreases with decreasing number of locations. However, if the depth and distance of the point sensor locations used for the profile shape correction extend down to at least 50 cm and are located within the minimum effective radius of the CRNS, one profile location can already improve results considerably (better than baseline performance), and with three profile locations, the reference performance is met. Between a linear vertical weighting and a more refined exponential vertical weighting (also depending on other field site conditions), no clear difference could be found.

When looking in detail at the soil moisture dynamics, the results confirm the satisfactory performance of the profile shape correction. However, we also identified periods, when the weighting approach does not improve the comparison, neither when using soil moisture network nor profile shape correction. The reason is attributed to a strong soil moisture gradient within the drying profile during these periods. Further research should be conducted to better understand these deviations and evaluate the performance of the weighting function for these cases.

Finally, results from the bias performance show that considering both the weighting and AHP is equally important. The former is especially important when considering performance measures assessing the time series dynamics. The latter can become more important for long-term experiments or cropped fields where AHP dynamics should be expected as well.

In conclusion, when CRNS is intended to be used as a method to monitor soil moisture, we recommend to additionally install a small measurement cluster with one to three additional point soil moisture sensor profiles and apply the profile shape correction as demonstrated in our study. Results from the four experimental datasets lead to the recommendation to install the additional soil moisture profiles down to a depth of 50 cm and within a radius of 100 m around the CRNS.

Although this additional installation may decrease the practical advantage of using CRNS as a noninvasive and stand-alone method, the corrected CRNS-derived soil moisture as deprived of the inherent weighting in the signal is more straightforward to interpret. The corrected CRNS-derived soil moisture better represents the mean soil moisture of its support volume and should perform better when used as direct input (e.g., top soil storage) for hydrologic models or for estimation of water fluxes (Dimitrova-Petrova et al., 2020; Franz et al., 2020; Nguyen et al., 2019; Peterson et al., 2016). These hypotheses should be tested in future studies. Deploying a few additional in situ soil moisture sensors that accompany the CRNS have additional advantages, as the contribution of biomass, interception, and ponding can be better assessed by using a simple scaling function (Baroni & Oswald, 2015; Nguyen et al., 2017). Further, the profile measurements might be used to derive depth-specific estimates from the integral CRNS soil moisture, which could be of interest for specific model applications. The proposed profile shape correction method might also be applicable for other proximal soil moisture sensing methods, such as gamma-ray spectroscopy (Baldoncini et al., 2018; Strati et al., 2018), because its signal is governed by a similar sensitivity as that of CRNS. Further research could also be conducted to identify alternative, less invasive approaches to estimate the soil moisture profile and use them to implement the profile shape correction.

CONFLICT OF INTEREST

The authors declare no conflict of interest.

AUTHOR CONTRIBUTION

L.S., G.B., and S.E.O. collected and analyzed the CRNS data for the field site KAT. T.F. delivered soil moisture and supporting data for SRER and HOAL, and J.J. did the same for SEL. L.S. analyzed the provided data and wrote and revised the manuscript. G.B., S.E.O., J.J., and T.F. contributed to the text and revised the manuscript. All authors approved the final manuscript.

ACKNOWLEDGMENTS

Funding for Lena Scheiffele and Jannis Jakobi was provided by DFG FOR-2694. We thank Joachim Ingwersen for providing the soil moisture sensor network data and additional information for the dataset KAT. This research was partly conceived during the IAEA Coordinated Research Project (CRP) "Enhancing agricultural resilience and water security using Cosmic-Ray Neutron Sensor" (D1.20.14)." We also acknowledge the contribution of the Hydrological Open Air Laboratory, who collected the dataset in Petzenkirchen (HOAL), the COsmic-ray Soil Moisture Observing System (COSMOS), who provided further data used within this study, the

TERrestrial Environmental Observatories (TERENO) funded by the Helmholtz-Gemeinschaft, who provided infrastructure for the SEL site, and the NMDB database funded by EU-FP7.

Open access funding enabled and organized by Projekt DEAL.

ORCID

Lena M. Scheiffele https://orcid.org/0000-0003-3621-680X
Gabriele Baroni https://orcid.org/0000-0003-2873-7162
Trenton E. Franz https://orcid.org/0000-0003-2947-0906
Jannis Jakobi https://orcid.org/0000-0002-3695-010X
Sascha E. Oswald https://orcid.org/0000-0003-1667-0060

REFERENCES

Andreasen, M., Jensen, K. H., Desilets, D., Franz, T. E., Zreda, M., Bogena, H. R., & Looms, M. C. (2017). Status and perspectives on the cosmic-ray neutron method for soil moisture estimation and other environmental science applications. *Vadose Zone J*, *16*(8). https://doi.org/10.2136/vzj2017.04.0086

Andreasen, M., Jensen, K. H., Desilets, D., Zreda, M., Bogena, H. R., & Looms, M. C. (2017). Cosmic-ray neutron transport at a forest field site: The sensitivity to various environmental conditions with focus on biomass and canopy interception. *Hydrology and Earth System Sciences*, *21*, 1875–1894. https://doi.org/10.5194/hess-21-1875-2017

Avery, W. A., Finkenbiner, C., Franz, T. E., Wang, T., Nguy-Robertson, A. L., Suyker, A., … Muñoz-Arriola, F. (2016). Incorporation of globally available datasets into the roving cosmic-ray neutron probe method for estimating field-scale soil water content. *Hydrology and Earth System Sciences*, *20*, 3859–3872. https://doi.org/10.5194/hess-20-3859-2016

Baatz, R., Bogena, H. R., Hendricks Franssen, H.-J., Huisman, J. A., Montzka, C., & Vereecken, H. (2015). An empirical vegetation correction for soil water content quantification using cosmic ray probes. *Water Resources Research*, *51*, 2030–2046. https://doi.org/10.1002/2014WR016443

Baatz, R., Bogena, H. R., Hendricks Franssen, H.-J., Huisman, J. A., Qu, W., Montzka, C., & Vereecken, H. (2014). Calibration of a catchment scale cosmic-ray probe network: A comparison of three parameterization methods. *Journal of Hydrology*, *516*, 231–244. https://doi.org/10.1016/j.jhydrol.2014.02.026

Baatz, R., Hendricks Franssen, H. J., Han, X., Hoar, T., Bogena, H. R., & Vereecken, H. (2017). Evaluation of a cosmic-ray neutron sensor network for improved land surface model prediction. *Hydrology and Earth System Sciences*, *21*, 2509–2530. https://doi.org/10.5194/hess-21-2509-2017

Baldoncini, M., Albéri, M., Bottardi, C., Chiarelli, E., Raptis, K. G. C., Strati, V., & Mantovani, F. (2018). Investigating the potentialities of Monte Carlo simulation for assessing soil water content via proximal gamma-ray spectroscopy. *Journal of Environmental Radioactivity*, *192*, 105–116. https://doi.org/10.1016/j.jenvrad.2018.06.001

Barker, J. B., Franz, T. E., Heeren, D. M., Neale, C. M. U., & Luck, J. D. (2017). Soil water content monitoring for irrigation management: A geostatistical analysis. *Agricultural Water Management*, *188*, 36–49. https://doi.org/10.1016/j.agwat.2017.03.024

Baroni, G., Ortuani, B., Facchi, A., & Gandolfi, C. (2013). The role of vegetation and soil properties on the spatio-temporal variability of the surface soil moisture in a maize-cropped field. *Journal of Hydrology*, *489*, 148–159. https://doi.org/10.1016/j.jhydrol.2013.03.007

Baroni, G., & Oswald, S. E. (2015). A scaling approach for the assessment of biomass changes and rainfall interception using cosmic-ray neutron sensing. *Journal of Hydrology*, *525*, 264–276. https://doi.org/10.1016/j.jhydrol.2015.03.053

Baroni, G., Scheiffele, L. M., Schrön, M., Ingwersen, J., & Oswald, S. E. (2018). Uncertainty, sensitivity and improvements in soil moisture estimation with cosmic-ray neutron sensing. *Journal of Hydrology*, *564*, 873–887. https://doi.org/10.1016/j.jhydrol.2018.07.053

Bogena, H. R., Herbst, M., Huisman, J. A., Rosenbaum, U., Weuthen, A., & Vereecken, H. (2010). Potential of wireless sensor networks for measuring soil water content variability. *Vadose Zone Journal*, *9*, 1002–1013. https://doi.org/10.2136/vzj2009.0173

Bogena, H. R., Huisman, J. A., Baatz, R., Hendricks Franssen, H. J., & Vereecken, H. (2013). Accuracy of the cosmic-ray soil water content probe in humid forest ecosystems: The worst case scenario. *Water Resources Research*, *49*, 5778–5791. https://doi.org/10.1002/wrcr.20463

Bogena, H. R., Montzka, C., Huisman, J. A., Graf, A., Schmidt, M., Stockinger, M., … Vereecken, H. (2018). The TERENO-Rur hydrological observatory: A multiscale multi-compartment research platform for the advancement of hydrological science. *Vadose Zone Journal*, *17*(1). https://doi.org/10.2136/vzj2018.03.0055

Brocca, L., Ciabatta, L., Massari, C., Camici, S., & Tarpanelli, A. (2017). Soil moisture for hydrological applications: Open questions and new opportunities. *Water*, *9*(2). https://doi.org/10.3390/w9020140

Brocca, L., Melone, F., Moramarco, T., & Morbidelli, R. (2010). Spatial-temporal variability of soil moisture and its estimation across scales. *Water Resources Research*, *46*(2). https://doi.org/10.1029/2009WR008016

Brocca, L., Ponziani, F., Moramarco, T., Melone, F., Berni, N., & Wagner, W. (2012). Improving landslide forecasting using ASCAT-derived soil moisture data: A case study of the Torgiovannetto landslide in central Italy. *Remote Sensing*, *4*, 1232–1244. https://doi.org/10.3390/rs4051232

Cabaniss, S. E., Madey, G., Leff, L., Maurice, P. A., & Wetzel, R. (2005). A stochastic model for the synthesis and degradation of natural organic matter. Part I. Data structures and reaction kinetics. *Biogeochemistry*, *76*, 319–347. https://doi.org/10.1007/s10533-005-6895-z

Cai, J., Pang, Z., & Fu, J. (2018). Spatial feature analysis of a cosmic-ray sensor for measuring the soil water content: Comparison of four weighting methods. *Physics and Chemistry of the Earth, Parts A/B/C*, *104*, 28–38. https://doi.org/10.1016/j.pce.2018.02.001

Chai, T., & Draxler, R. R. (2014). Root mean square error (RMSE) or mean absolute error (MAE)?: Arguments against avoiding RMSE in the literature. *Geoscientific Model Development*, *7*, 1247–1250. https://doi.org/10.5194/gmd-7-1247-2014

Chatterjee, A., Lal, R., Wielopolski, L., Martin, M. Z., & Ebinger, M. H. (2009). Evaluation of different soil carbon determination methods. *Critical Reviews in Plant Sciences*, *28*, 164–178. https://doi.org/10.1080/07352680902776556

Chrisman, B., & Zreda, M. (2013). Quantifying mesoscale soil moisture with the cosmic-ray rover. *Hydrology and Earth System Sciences*, *17*, 5097–5108. https://doi.org/10.5194/hess-17-5097-2013

Coopersmith, E. J., Cosh, M. H., & Daughtry, C. S. T. (2014). Field-scale moisture estimates using COSMOS sensors: A validation study with

temporary networks and leaf-area-indices. *Journal of Hydrology*, *519*, 637–643. https://doi.org/10.1016/j.jhydrol.2014.07.060

Corradini, C. (2014). Soil moisture in the development of hydrological processes and its determination at different spatial scales. *Journal of Hydrology*, *516*, 1–5. https://doi.org/10.1016/j.jhydrol.2014.02.051

Davies, B. E. (1974). Loss-on-ignition as an estimate of soil organic matter. *Soil Science Society of America Journal*, *38*, 150–151. https://doi.org/10.2136/sssaj1974.03615995003800010046x

Desilets, D., Zreda, M., & Ferré, T. P. A. (2010). Nature's neutron probe: Land surface hydrology at an elusive scale with cosmic rays. *Water Resources Research*, *46*(11). https://doi.org/10.1029/2009WR008726.

Dimitrova-Petrova, K., Geris, J., Mark Wilkinson, E., Rosolem, R., Verrot, L., Lilly, A., & Soulsby, C. (2020). Opportunities and challenges in using catchment-scale storage estimates from cosmic ray neutron sensors for rainfall-runoff modelling. *Journal of Hydrology*, *586*, 124878. https://doi.org/10.1016/j.jhydrol.2020.124878

Dong, J., Ochsner, T. E., Zreda, M., Cosh, M. H., & Zou, C. B. (2014). Calibration and validation of the COSMOS rover for surface soil moisture measurement. *Vadose Zone Journal*, *13*(4). https://doi.org/10.2136/vzj2013.08.0148

Dunai, T. J. (2000). Scaling factors for production rates of in situ produced cosmogenic nuclides: A critical reevaluation. *Earth and Planetary Science Letters*, *176*, 157–169. https://doi.org/10.1016/S0012-821X(99)00310-6

Duygu, M. B., & Akyürek, Z. (2019). Using cosmic-ray neutron probes in validating satellite soil moisture products and land surface models. *Water*, *11*(7). https://doi.org/10.3390/w11071362

Evans, J. G., Ward, H. C., Blake, J. R., Hewitt, E. J., Morrison, R., Fry, M., … Jenkins, A. (2016). Soil water content in southern England derived from a cosmic-ray soil moisture observing system—COSMOS-UK. *Hydrological Processes*, *30*, 4987–4999. https://doi.org/10.1002/hyp.10929

Fersch, B., Francke, T., Heistermann, M., Schrön, M., Döpper, V., Jakobi, J., … Oswald, S. (2020). A dense network of cosmic-ray neutron sensors for soil moisture observation in a highly instrumented pre-Alpine headwater catchment in Germany. *Earth System Science Data*, *12*, 2289–2309. https://doi.org/10.5194/essd-12-2289-2020

Fersch, B., Jagdhuber, T., Schrön, M., Völksch, I., & Jäger, M. (2018). Synergies for soil moisture retrieval across scales from airborne polarimetric SAR, cosmic ray neutron roving, and an in situ sensor network. *Water Resources Research*, *54*, 9364–9383. https://doi.org/10.1029/2018WR023337

Finkenbiner, C. E., Franz, T. E., Gibson, J., Heeren, D. M., & Luck, J. (2019). Integration of hydrogeophysical datasets and empirical orthogonal functions for improved irrigation water management. *Precision Agriculture*, *20*, 78–100. https://doi.org/10.1007/s11119-018-9582-5

Franz, T. E., Wahbi, A., Vreugdenhil, M., Weltin, G., Heng, L., Oismueller, M., … Desilets, D. (2016). Using cosmic-ray neutron probes to monitor landscape scale soil water content in mixed land use agricultural systems. *Applied and Environmental Soil Science*, *2016*. https://doi.org/10.1155/2016/4323742

Franz, T. E., Wahbi, A., Zhang, J., Vreugdenhil, M., Heng, L., Dercon, G., … Wagner, W. (2020). Practical data products from cosmic-ray neutron sensing for hydrological applications. *Frontiers in Water*, *2*, https://doi.org/10.3389/frwa.2020.00009

Franz, T. E., Wang, T., Avery, W., Finkenbiner, C., & Brocca, L. (2015). Combined analysis of soil moisture measurements from roving and fixed cosmic ray neutron probes for multiscale real-time monitoring. *Geophysical Research Letters*, *42*, 3389–3396. https://doi.org/10.1002/2015GL063963

Franz, T. E., Zreda, M., Ferre, T. P. A., & Rosolem, R. (2013). An assessment of the effect of horizontal soil moisture heterogeneity on the area-average measurement of cosmic-ray neutrons. *Water Resources Research*, *49*, 6450–6458. https://doi.org/10.1002/wrcr.20530

Franz, T. E., Zreda, M., Ferre, T. P. A., Rosolem, R., Zweck, C., Stillman, S., … Shuttleworth, W. J. (2012). Measurement depth of the cosmic ray soil moisture probe affected by hydrogen from various sources. *Water Resources Research*, *48*(8). https://doi.org/10.1029/2012WR011871

Franz, T. E., Zreda, M., Rosolem, R., & Ferre, T. P. A. (2012). Field validation of a cosmic-ray neutron sensor using a distributed sensor network. *Vadose Zone Journal*, *11*(4). https://doi.org/10.2136/vzj2012.0046

Franz, T. E., Zreda, M., Rosolem, R., & Ferre, T. P. A. (2013b). A universal calibration function for determination of soil moisture with cosmic-ray neutrons. *Hydrology and Earth System Sciences*, *17*, 453–460. https://doi.org/10.5194/hess-17-453-2013

Franz, T. E., Zreda, M., Rosolem, R., Hornbuckle, B. K., Irvin, S. L., Adams, H., … Shuttleworth, W. J. (2013). Ecosystem-scale measurements of biomass water using cosmic ray neutrons. *Geophysical Research Letters*, *40*, 3929–3933. https://doi.org/10.1002/grl.50791

Han, X., Hendricks Franssen, H. J., Jiménez Bello, M. Á., Rosolem, R., Bogena, H., Alzamora, F. M., & Vereecken, H. (2016). Simultaneous soil moisture and properties estimation for a drip irrigated field by assimilating cosmic-ray neutron intensity. *Journal of Hydrology*, *539*, 611–624. https://doi.org/10.1016/j.jhydrol.2016.05.050

Hawdon, A., McJannet, D., & Wallace, J. (2014). Calibration and correction procedures for cosmic-ray neutron soil moisture probes located across Australia. *Water Resources Research*, *50*, 5029–5043. https://doi.org/10.1002/2013WR015138

Heidbüchel, I., Güntner, A., & Blume, T. (2016). Use of cosmic-ray neutron sensors for soil moisture monitoring in forests. *Hydrology and Earth System Sciences*, *20*, 1269–1288. https://doi.org/10.5194/hess-20-1269-2016

Huang, C., Marsh, S. E., McClaran, M. P., & Archer, S. R. (2007). Postfire stand structure in a semiarid savanna: Cross-scale challenges estimating biomass. *Ecological Applications*, *17*, 1899–1910. https://doi.org/10.1890/06-1968.1

Hupet, F., & Vanclooster, M. (2002). Intraseasonal dynamics of soil moisture variability within a small agricultural maize cropped field. *Journal of Hydrology*, *261*, 86–101. https://doi.org/10.1016/S0022-1694(02)00016-1

Imukova, K., Ingwersen, J., Hevart, M., & Streck, T. (2016). Energy balance closure on a winter wheat stand: Comparing the eddy covariance technique with the soil water balance method. *Biogeosciences*, *13*, 63–75. https://doi.org/10.5194/bg-13-63-2016

Iwema, J., Rosolem, R., Baatz, R., Wagener, T., & Bogena, H. R. (2015). Investigating temporal field sampling strategies for site-specific calibration of three soil moisture–neutron intensity parameterisation methods. *Hydrology and Earth System Sciences*, *19*, 3203–3216. https://doi.org/10.5194/hess-19-3203-2015

Iwema, J., Rosolem, R., Rahman, M., Blyth, E., & Wagener, T. (2017). Land surface model performance using cosmic-ray and point-scale soil moisture measurements for calibration. *Hydrology and Earth System Sciences*, *21*, 2843–2861. https://doi.org/10.5194/hess-21-2843-2017

Jakobi, J. C., Huisman, J. A., Schrön, M., Fiedler, J. E., Brogi, C., Vereecken, H., & Bogena, H. R. (2020). Error estimation for soil moisture measurements with cosmic ray neutron sensing and implications for rover surveys. *Frontiers in Water*, *2*. https://doi.org/10.3389/frwa.2020.00010.

Jakobi, J., Huisman, J. A., Vereecken, H., Diekkrüger, B., & Bogena, H. R. (2018). Cosmic ray neutron sensing for simultaneous soil water content and biomass quantification in drought conditions. *Water Resources Research*, *54*, 7383–7402. https://doi.org/10.1029/2018WR022692

Jensen, J. L., Christensen, B. T., Schjønning, P., Watts, C. W., & Munkholm, L. J. (2018). Converting loss-on-ignition to organic carbon content in arable topsoil: Pitfalls and proposed procedure. *European Journal of Soil Science*, *69*, 604–612. https://doi.org/10.1111/ejss.12558

Knoben, W. J. M., Freer, J. E., & Woods, R. A. (2019). Technical note: Inherent benchmark or not? Comparing Nash–Sutcliffe and Kling–Gupta efficiency scores. *Hydrology and Earth System Sciences*, *23*, 4323–4331. https://doi.org/10.5194/hess-23-4323-2019

Köhli, M., Schrön, M., Zreda, M., Schmidt, U., Dietrich, P., & Zacharias, S. (2015). Footprint characteristics revised for field-scale soil moisture monitoring with cosmic-ray neutrons. *Water Resources Research*, *51*, 5772–5790. https://doi.org/10.1002/2015WR017169

Koster, R. D., Mahanama, S. P. P., Livneh, B., Lettenmaier, D. P., & Reichle, R. H. (2010). Skill in streamflow forecasts derived from large-scale estimates of soil moisture and snow. *Nature Geoscience*, *3*, 613–616. https://doi.org/10.1038/ngeo944

Lv, L., Franz, T. E., Robinson, D. A., & Jones, S. B. (2014). Measured and modeled soil moisture compared with cosmic-ray neutron probe estimates in a mixed forest. *Vadose Zone Journal*, *13*(12). https://doi.org/10.2136/vzj2014.06.0077

McJannet, D., Hawdon, A., Baker, B., Renzullo, L., & Searle, R. (2017). Multiscale soil moisture estimates using static and roving cosmic-ray soil moisture sensors. *Hydrology and Earth System Sciences*, *21*, 6049–6067. https://doi.org/10.5194/hess-21-6049-2017

Montzka, C., Bogena, H. R., Zreda, M., Monerris, A., Morrison, R., Muddu, S., & Vereecken, H. (2017). Validation of spaceborne and modelled surface soil moisture products with cosmic-ray neutron probes. *Remote Sensing*, *9*(2). https://doi.org/10.3390/rs9020103

Nelson, D. W., & Sommers, L. E. (1996). Total carbon, organic carbon, and organic matter. In D. L. Sparks, et al. (Eds.), *Methods of soil analysis. Part 3. Chemical methods* (pp. 961–1010). Madison, WI: SSSA and ASA. https://doi.org/10.2136/sssabookser5.3.c34

Nguyen, H. H., Jeong, J., & Choi, M. (2019). Extension of cosmic-ray neutron probe measurement depth for improving field scale root-zone soil moisture estimation by coupling with representative in-situ sensors. *Journal of Hydrology*, *571*, 679–696. https://doi.org/10.1016/j.jhydrol.2019.02.018

Nguyen, H. H., Kim, H., & Choi, M. (2017). Evaluation of the soil water content using cosmic-ray neutron probe in a heterogeneous monsoon climate-dominated region. *Advances in Water Resources*, *108*, 125–138. https://doi.org/10.1016/j.advwatres.2017.07.020

Ochsner, T. E., Cosh, M. H., Cuenca, R. H., Dorigo, W. A., Draper, C. S., Hagimoto, Y., … Zreda, M. (2013). State of the art in large-scale soil moisture monitoring. *Soil Science Society of America Journal*, *77*, 1888–1919. https://doi.org/10.2136/sssaj2013.03.0093

Pendergrass, A. G., Meehl, G. A., Pulwarty, R., Hobbins, M., Hoell, A., AghaKouchak, A., … Woodhouse, C. A. (2020). Flash droughts present a new challenge for subseasonal-to-seasonal prediction. *Nature Climate Change*, *10*, 191–199. https://doi.org/10.1038/s41558-020-0709-0

Peterson, A. M., Helgason, W. D., & Ireson, A. M. (2016). Estimating field-scale root zone soil moisture using the cosmic-ray neutron probe. *Hydrology and Earth System Sciences*, *20*, 1373–1385. https://doi.org/10.5194/hess-20-1373-2016

Picciafuoco, T., Morbidelli, R., Flammini, A., Saltalippi, C., Corradini, C., Strauss, P., & Blöschl, G. (2019). On the estimation of spatially representative plot scale saturated hydraulic conductivity in an agricultural setting. *Journal of Hydrology*, *570*, 106–117. https://doi.org/10.1016/j.jhydrol.2018.12.044

Pribyl, D. W. (2010). A critical review of the conventional SOC to SOM conversion factor. *Geoderma*, *156*, 75–83. https://doi.org/10.1016/j.geoderma.2010.02.003

Ragab, R., Evans, J. G., Battilani, A., & Solimando, D. (2017). The Cosmic-ray Soil Moisture Observation System (COSMOS) for estimating the crop water requirement: New approach. *Irrigation and Drainage*, *66*, 456–468. https://doi.org/10.1002/ird.2152

Rivera Villarreyes, C. A., Baroni, G., & Oswald, S. E. (2011). Integral quantification of seasonal soil moisture changes in farmland by cosmic-ray neutrons. *Hydrology and Earth System Sciences*, *15*, 3843–3859. https://doi.org/10.5194/hess-15-3843-2011

Robinson, D. A., Campbell, C. S., Hopmans, J. W., Hornbuckle, B. K., Jones, S. B., Knight, R., … Wendroth, O. (2008). Soil moisture measurement for ecological and hydrological watershed-scale observatories: A review. *Vadose Zone Journal*, *7*, 358–389. https://doi.org/10.2136/vzj2007.0143

Rosolem, R., Hoar, T., Arellano, A., Anderson, J. L., Shuttleworth, W. J., Zeng, X., & Franz, T. E. (2014). Translating aboveground cosmic-ray neutron intensity to high-frequency soil moisture profiles at sub-kilometer scale. *Hydrology and Earth System Sciences*, *18*, 4363–4379. https://doi.org/10.5194/hess-18-4363-2014

Rosolem, R., Shuttleworth, W. J., Zreda, M., Franz, T. E., Zeng, X., & Kurc, S. A. (2013). The effect of atmospheric water vapor on neutron count in the cosmic-ray soil moisture observing system. *Journal of Hydrometeorology*, *14*, 1659–1671. https://doi.org/10.1175/JHM-D-12-0120.1

Rudolph, S., van der Kruk, J., von Hebel, C., Ali, M., Herbst, M., Montzka, C., … Weihermüller, L. (2015). Linking satellite derived LAI patterns with subsoil heterogeneity using large-scale ground-based electromagnetic induction measurements. *Geoderma*, *241–242*, 262–271. https://doi.org/10.1016/j.geoderma.2014.11.015

Schreiner-McGraw, A. P., Vivoni, E. R., Mascaro, G., & Franz, T. E. (2016). Closing the water balance with cosmic-ray soil moisture measurements and assessing their relation to evapotranspiration in two semiarid watersheds. *Hydrology and Earth System Sciences*, *20*, 329–345. https://doi.org/10.5194/hess-20-329-2016

Schrön, M., Köhli, M., Scheiffele, L., Iwema, J., Bogena, H. R., Lv, L., … Zacharias, S. (2017). Improving calibration and validation of cosmic-ray neutron sensors in the light of spatial sensitivity. *Hydrology and Earth System Sciences*, *21*, 5009–5030. https://doi.org/10.5194/hess-21-5009-2017

Schrön, M., Rosolem, R., Köhli, M., Piussi, L., Schröter, I., Iwema, J., … Zacharias, S. (2018). Cosmic-ray neutron rover surveys of field soil moisture and the influence of roads. *Water Resources Research*, *54*, 6441–6459. https://doi.org/10.1029/2017WR021719

Schrön, M., Zacharias, S., Womack, G., Köhli, M., Desilets, D., Oswald, S. E., … Dietrich, P. (2018). Intercomparison of cosmic-ray

neutron sensors and water balance monitoring in an urban environment. *Geoscientific Instrumentation, Methods and Data Systems*, *7*, 83–99. https://doi.org/10.5194/gi-7-83-2018

Seneviratne, S. I., Corti, T., Davin, E. L., Hirschi, M., Jaeger, E. B., Lehner, I., … Teuling, A. J. (2010). Investigating soil moisture–climate interactions in a changing climate: A review. *Earth-Science Reviews*, *99*, 125–161. https://doi.org/10.1016/j.earscirev.2010.02.004

Shrestha, P., & Simmer, C. (2020). Modeled land atmosphere coupling response to soil moisture changes with different generations of land surface models. *Water*, *12*(1). https://doi.org/10.3390/w12010046

Shuttleworth, J., Rosolem, R., Zreda, M., & Franz, T. (2013). The COsmic-ray Soil Moisture Interaction Code (COSMIC) for use in data assimilation. *Hydrology and Earth System Sciences*, *17*, 3205–3217. https://doi.org/10.5194/hess-17-3205-2013

Sigouin, M. J. P., Dyck, M., Si, B. C., & Hu, W. (2016). Monitoring soil water content at a heterogeneous oil sand reclamation site using a cosmic-ray soil moisture probe. *Journal of Hydrology*, *543*, 510–522. https://doi.org/10.1016/j.jhydrol.2016.10.026

Strati, V., Albéri, M., Anconelli, S., Baldoncini, M., Bittelli, M., Bottardi, C., … Mantovani, F. (2018). Modelling soil water content in a tomato field: Proximal gamma ray spectroscopy and soil–crop system models. *Agriculture*, *8*(4). https://doi.org/10.3390/agriculture8040060

Teuling, A. J., Uijlenhoet, R., Hupet, F., van Loon, E. E., & Troch, P. A. (2006). Estimating spatial mean root-zone soil moisture from point-scale observations. *Hydrology and Earth System Sciences*, *10*, 755–767. https://doi.org/10.5194/hess-10-755-2006

Tian, Z., Li, Z., Liu, G., Li, B., & Ren, T. (2016). Soil water content determination with cosmic-ray neutron sensor: Correcting aboveground hydrogen effects with thermal/fast neutron ratio. *Journal of Hydrology*, *540*, 923–933. https://doi.org/10.1016/j.jhydrol.2016.07.004

Vanderlinden, K., Vereecken, H., Hardelauf, H., Herbst, M., Martínez, G., Cosh, M. H., & Pachepsky, Y. A. (2012). Temporal stability of soil water contents: A review of data and analyses. *Vadose Zone Journal*, *11*(4). https://doi.org/10.2136/vzj2011.0178

Vereecken, H., Huisman, J. A., Pachepsky, Y., Montzka, C., van der Kruk, J., Bogena, H., … Vanderborght, J. (2014). On the spatio-temporal dynamics of soil moisture at the field scale. *Journal of Hydrology*, *516*, 76–96. https://doi.org/10.1016/j.jhydrol.2013.11.061.

Wang, E., Smith, C. J., Macdonald, B. C. T., Hunt, J. R., Xing, H., Denmead, O. T., … Isaac, P. (2018). Making sense of cosmic-ray soil moisture measurements and eddy covariance data with regard to crop water use and field water balance. *Agricultural Water Management*, *204*, 271–280. https://doi.org/10.1016/j.agwat.2018.04.017

Wehrli, K., Guillod, B. P., Hauser, M., Leclair, M., & Seneviratne, S. I. (2019). Identifying key driving processes of major recent heat waves. *JGR Atmospheres*, *124*, 11746–11765. https://doi.org/10.1029/2019JD030635

Wuest, S. (2014). Seasonal variation in soil organic carbon. *Soil Science Society of America Journal*, *78*, 1442–1447. https://doi.org/10.2136/sssaj2013.10.0447

Wuest, S. B. (2015). Seasonal variation in soil bulk density, organic nitrogen, available phosphorus, and pH. *Soil Science Society of America Journal*, *79*, 1188–1197. https://doi.org/10.2136/sssaj2015.02.0066

Zhu, X., Shao, M., Jia, X., Huang, L., Zhu, J., & Zhang, Y. (2017). Application of temporal stability analysis in depth-scaling estimated soil water content by cosmic-ray neutron probe on the northern Tibetan Plateau. *Journal of Hydrology*, *546*, 299–308. https://doi.org/10.1016/j.jhydrol.2017.01.019

Zreda, M., Desilets, D., Ferré, T. P. A., & Scott, R. L. (2008). Measuring soil moisture content non-invasively at intermediate spatial scale using cosmic-ray neutrons. *Geophysical Research Letters*, *35*(21). https://doi.org/10.1029/2008GL035655

Zreda, M., Shuttleworth, W. J., Zeng, X., Zweck, C., Desilets, D., Franz, T., & Rosolem, R. (2012). COSMOS: The COsmic-ray soil moisture observing system. *Hydrology and Earth System Sciences*, *16*, 4079–4099. https://doi.org/10.5194/hess-16-4079-2012

How to cite this article: Scheiffele LM, Baroni G, Franz TE, Jakobi J, Oswald SE. A profile shape correction to reduce the vertical sensitivity of cosmic-ray neutron sensing of soil moisture. *Vadose Zone J.* 2020;19:e20083. https://doi.org/10.1002/vzj2.20083

APPENDIX

A | Corrections of raw neutron counts

The raw neutron counts (N_{raw}, counts per hour) as detected by the probe have to be corrected for variations in pressure (P_{atm}, mbar), incoming radiation (N_{inc}, counts per hour), and air humidity (h_{air}, g cm^{-3}):

$$N = N_{raw} \cdot \exp\left(\frac{P_{atm} - P_{atm}^{ref}}{\Lambda}\right) \cdot \left(\frac{N_{inc}^{ref}}{N_{inc}}\right) \cdot \left[1 + 0.0054\left(h_{air} - h_{air}^{ref}\right)\right] \quad \text{(A1)}$$

where Λ is the attenuation length (mbar; for calculation, refer to Dunai, 2000) and the reference values for air pressure and incoming radiation (P_{atm}^{ref}, N_{inc}^{ref}) are usually the mean over the measurement period and the reference value for air humidity (h_{air}^{ref}) is set to 0 g m^{-3} (Bogena et al., 2013; Rosolem et al., 2013; Zreda et al., 2012).

B | Additional soil hydrogen pools

Organic matter consists of different compounds like humic acids and celluloses or lignin. The ratio of oxygen and hydrogen contained in organic matter is approximately the same as in a water molecule, and the weight fraction of this soil water equivalent (SOW) is approximately the same weight percentage as the carbon fraction (Cabaniss, Madey, Leff, Maurice, & Wetzel, 2005; Nelson & Sommers, 1996; Pribyl, 2010). Thus, either organic carbon can be determined (e.g., with dry combustion; Chatterjee, Lal, Wielopolski, Martin, & Ebinger, 2009), or organic matter (OM) of a soil can be determined by the loss-on-ignition method (400 ˚C, 16 h; Davies, 1974; Jensen, Christensen, Schjønning, Watts, & Munkholm, 2018). Then, the weight fraction of water

equivalent (SOW, g g^{-1}) can be determined by

$$SOW = \frac{OM}{2}$$

The traditional conversion factor of 1.724 is not appropriate and should not be used anymore (Pribyl, 2010).

Lattice water (LW, g g^{-1}) is determined by loss-on-ignition by heating soil samples to 1,000 ˚C (after having removed organic matter to avoid measuring the decomposition of both) for 12 h (Zreda et al., 2012). In this study, the two additional soil hydrogen pools are assumed to be static and are converted to volumetric additional soil hydrogen pools AHP (m^3 m^{-3}) by multiplying them with the bulk density ρ_b (g cm^{-3}) of the soils.

C | Rescaled radius and horizontal weighting

The rescaled radius used for the calculation of the penetration depth D_{86} and used in the horizontal weighting is calculated by applying a pressure and a vegetation correction:

$$r^* = \frac{r}{f_p / f_{veg}}$$

$$f_p = \frac{0.5}{0.86 - e^{-P_{atm}/P_{ref}}}$$

$$f_{veg} = 1 - 0.17\left(1 - e^{-0.41 h_{veg}}\right)\left(1 + e^{-9.25\theta_p}\right)$$

P_{ref} is the standard atmospheric pressure at sea level (1,013.25 mbar), P_{atm} the measured atmospheric pressure. h_{veg} is the vegetation height (cm). The θ_p is the equally weighted soil moisture for the calculation of D_{86}, and for the calculation of horizontal weights, it is the depth-weighted soil moisture of each location.

The horizontal weighting of depth weighted profile soil moisture follows the procedure described in Köhli et al. (2015) and Schrön et al. (2017)

$$wt(r) = \begin{cases} F_1 e^{-F_2 r^*} + F_3 e^{-F_4 r^*}, & 1\text{m} < r \leq 50\text{m} \\ F_5 e^{-F_6 r^*} + F_7 e^{-F_8 r^*}, & 50\text{m} < r < 600\text{m} \end{cases}$$

For parameter functions F_i and parameter values refer to Schrön et al. (2017). They also describe a weighting for distances 0 m $< r \leq$ 1 m, which is not applicable within this study, as no soil moisture sensors were placed this close to the CRNS.

D | Analysis using other performance measures

Table D1 lists all performance measures using maximum available locations and measurement depth for the four field sites. Results for RMSE and KGE are discussed in the main text (Section 3.1). In the same way as RMSE values are calculated within the main analysis, MAE, NSE, and KGE are calculated for a baseline performance [comparing $\theta_{SN(avg)}$ and θ_{CRNS}], assessing the bias introduced by AHP [bias performance, by comparing $\theta_{CRNS(vol)}$ with $\theta_{SN(avg)}$], for a reference performance [comparing $\theta_{SN(wt)}$ with θ_{CRNS}] and assessing the results from the profile shape correction for each of the measures ($RMSE_{pc}$, MAE_{pc}, NSE_{pc}, and KGE_{pc}).

Results for the MAE closely follow the results from RMSE, with MAE_{bias} ranging between MAE_{base} and MAE_{ref} and, except for HAOL, even further improvement in the measure for MAE_{pc}. For HOAL, the MAE for all comparisons are within a close range, different from MAEs at the other field sites. This is likely explained with a general shift between θ_{SN} and θ_{CRNS} over the measurement period that is attributed to biomass change and influence of agricultural management operations. The HOAL site also shows worse performance than the other field sites for the measures dealing with time series dynamics (NSE and KGE) for the reference performance and the profile shape correction. For HOAL, taking only the three locations within a radial distance $d \leq 100$ m leads to improved performance of the profile shape correction with 0.023 and 0.046 for NSE_{pc} and KGE_{pc}, respectively. Clearly NSE and KGE show that dealing with the weighting either of the sensor network [$\theta_{SN(wt)}$] as in the reference performance or the unweighting of CRNS as in the profile shape correction improves the time series dynamics.

Shown in Figures D1–D4, analogous to the analysis on RMSE in the main text, is a complete analysis of the profile shape correction using other performance measures for the field site KAT

For all performance measures, the same trend can be observed (Figure D1). Better and more stable values of the measures are achieved with increasing sample size. The systematic deviation due to the AHP is assessed with the bias performance, and according to the RMSE, the MAE explains approximately half of the improvement of the reference performance. The NSE and KGE show less and almost no improvement, respectively, for the bias performance compared with the baseline performance at this field site. Especially for the KGE, the improvement in performance is mostly explained by dealing with the weighting. Results from the profile shape correction reach the reference performance for RMSE and MAE. For KGE and NSE, the results of the profile shape correction stay between the reference and the bias performance.

As for the analysis for RMSE, best MAE_{pc} and NSE_{pc} are achieved for 50- to 60-cm depth. For KGE_{pc}, better results can be achieved for using measurement depth down to 70 cm (Figure D2).

Results from the analysis for radial distance for the other performance measures confirms results from the main analysis (Figure D3) for this field site.

Figure D4 shows the results of using one to three locations (k) within a distance of $r \leq 75$ m around the CRNS and

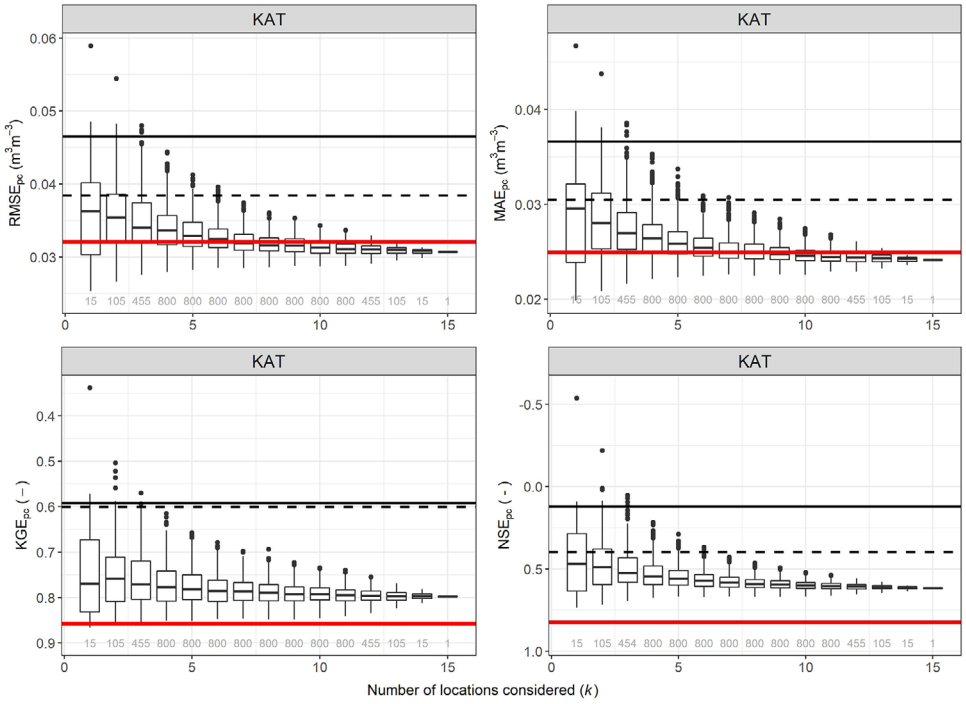

FIGURE D1 Comparison of the complete analysis for the performance measures for depth $d = 90$ cm, radial distance $r = 150$ m, and decreasing sample size k at the field site Katharinentaler Hof (KAT). Panels show the profile shape correction performance for root mean square error, mean absolute error, Kling–Gupta efficiency, and Nash–Sutcliffe efficiency ($RMSE_{pc}$, MAE_{pc}, KGE_{pc}, and NSE_{pc}). Baseline performance for each measure is marked as a black line, the reference performance is marked as a red line, and the bias performance is marked with a black and dashed line. The $RMSE_{pc}$ is the same as presented in Figure 2

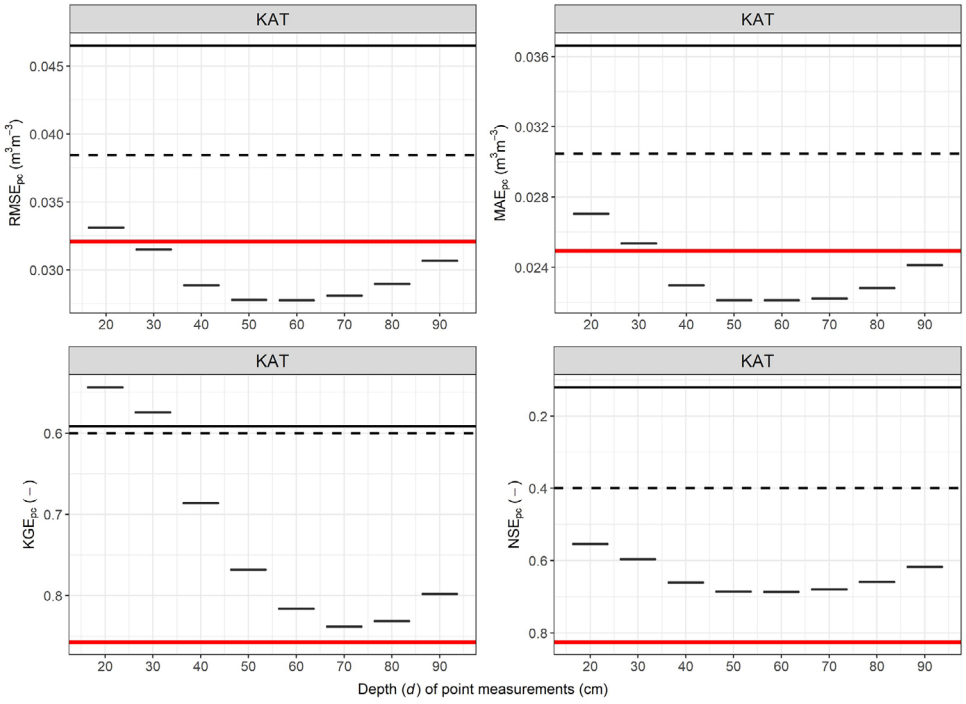

FIGURE D2 Results from the analysis for the influence of the measurement depth (d) for sample size $k = 15$ and radial distance $r = 150$ m at the field site Katharinentaler Hof (KAT). Panels show the profile shape correction performance for root mean square error, mean absolute error, Kling–Gupta efficiency, and Nash–Sutcliffe efficiency ($RMSE_{pc}$, MAE_{pc}, KGE_{pc}, and NSE_{pc}). Baseline performance for each measure is marked as a black line, the reference performance is marked as a red line, and the bias performance is marked with a black and dashed line. The $RMSE_{pc}$ is the same as presented in Figure 4.

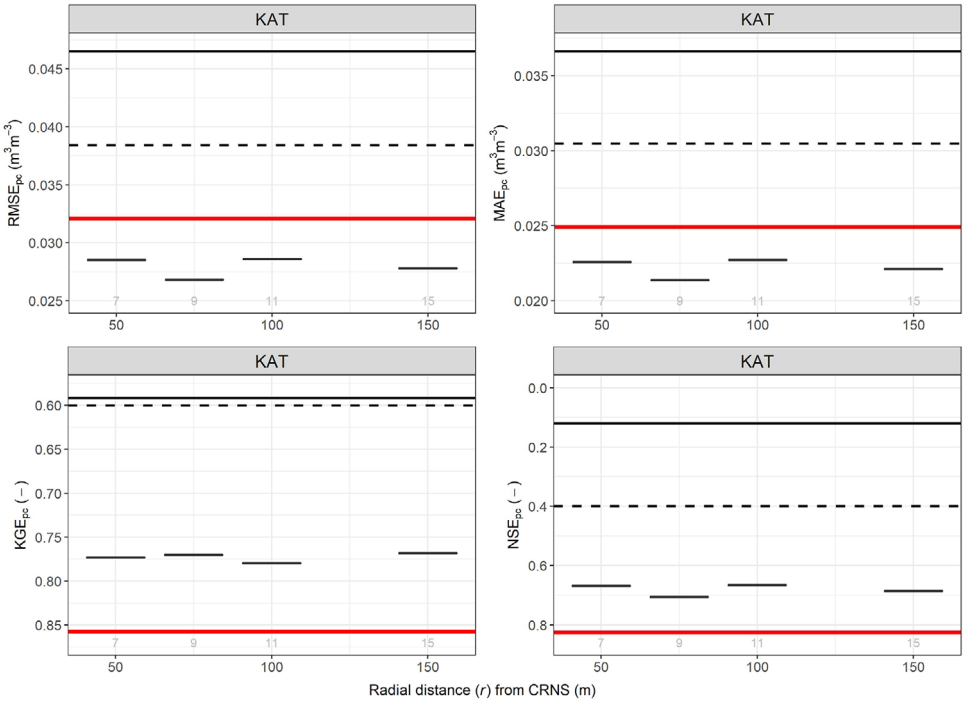

FIGURE D3 Results from the analysis for the influence of the radial distance (r) for $d = 50$ cm at the field site Katharinentaler Hof (KAT). Number of point locations (k) within the considered distances are given in grey numbers. Panels show the profile shape correction performance for root mean square error, mean absolute error, Kling–Gupta efficiency, and Nash–Sutcliffe efficiency (RMSE$_{pc}$, MAE$_{pc}$, KGE$_{pc}$, and NSE$_{pc}$). Baseline performance for each measure is marked as a black line, the reference performance is marked as a red line and the bias performance with a black and dashed line. The RMSE$_{pc}$ is the same as presented in Figure 5.

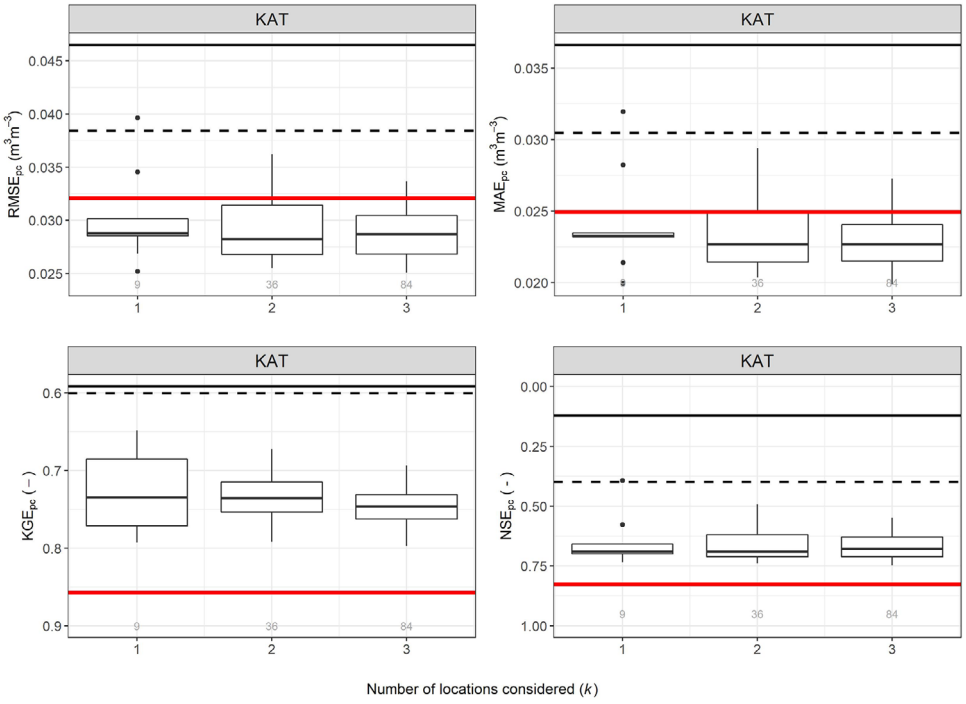

FIGURE D4 Comparison of the analysis for the performance measures for depth $d = 50$, radial distance $r = 75$, and sample size $k = 1$, 2, and 3 at the field site Katharinentaler Hof (KAT). Panels show the profile shape correction performance for root mean square error, mean absolute error, Kling–Gupta efficiency, and Nash–Sutcliffe efficiency (RMSE$_{pc}$, MAE$_{pc}$, KGE$_{pc}$, and NSE$_{pc}$). Baseline performance for each measure is marked as a black line, the reference performance is marked as a red line, and the bias performance is marked with a black and dashed line. The RMSE$_{pc}$ is the same as presented in Figure 6.

TABLE D1 The performance measures for all field sites. Baseline performance (base) compares average soil moisture from the sensor network [$\theta_{SN(avg)}$] and soil moisture derived from cosmic-ray neutron sensing (CRNS) (θ_{CRNS}). The bias performance (bias) assesses the influence of only subtracting additional hydrogen pools (AHP) from CRNS-derived soil moisture resulting in $\theta_{CRNS(vol)}$ (volumetric CRNS-derived soil moisture) and compares it with $\theta_{SN(avg)}$. For the reference performance (ref), the weighted sensor network, including AHP [$\theta_{SN(wt)}$] is compared with θ_{CRNS}, and the performance of the profile shape correction (pc) is assessed by comparing corrected CRNS-derived soil moisture [$\theta_{CRNS(pc)}$] with $\theta_{SN(avg)}$

Site[a]	Performance	RMSE	MAE[b]	NSE[c]	KGE[d]
		–m^3 m^{-3}–			
KAT	base	0.47	0.037	0.12	0.59
	bias	0.038	0.031	0.40	0.60
	ref	0.032	0.025	0.86	0.86
	pc[e]	0.031	0.024	0.62	0.80
HOAL	base	0.064	0.050	−0.13	0.44
	bias	0.059	0.049	0.02	0.45
	Ref	0.054	0.045	0.32	0.54
	pc[e]	0.059	0.048	0.04	0.23
SEL	base	0.066	0.059	0.17	0.58
	bias	0.046	0.036	0.52	0.66
	ref	0.046	0.036	0.58	0.70
	pc[e]	0.041	0.034	0.67	0.70
SRER	base	0.037	0.029	−4.07	−0.17
	bias	0.026	0.019	−1.50	−0.03
	Ref	0.019	0.013	0.47	0.68
	pc[e]	0.016	0.011	0.68	0.60

[a]KAT, Katharinentaler Hof; HOAL, Hydrological Open Air Laboratory; SEL, Selhausen; SRER, Santa Rita Experimental Range.
[b]MAE, mean absolute error.
[c]NSE, Nash–Sutcliffe efficiency.
[d]KGE, Kling–Gupta efficiency.
[e]Profile shape correction is based on different measurement depths, radial distances, and sample sizes (d, r, and k) for the field sites: KAT (90, 150, and 15), HOAL (50, 320, and 16), SEL (50, 100, and 18), and SRER (70, 200, and 18).

measurement depth $d \leq 50$ cm. As for the $RMSE_{pc}$, the MAE_{pc} reaches reference performance. For KGE_{pc} and NSE_{pc}, the results stay above reference performance but are clearly lower performance than only handling the systematic deviation of the AHP. Although the weighting introduces very similar dynamics in the sensor network [$\theta_{SN(wt)}$], as observed for the CRNS time series, the profile shape correction on CRNS-derived soil moisture does diminish some but not all of these dynamics in $\theta_{CRNS(pc)}$ (see Section 3.6 and Figure 8). This explains why the performance measures dealing with the time series dynamics (KGE and NSE) do not reach reference performance. However, in particular, results from KGE show that in terms of time series dynamics, dealing with the inherent weighting can be more important than subtracting AHP. Thus, even with slight differences as observed for measurement depth with the KGE (Figure D2), the analysis using other performance measures confirms results drawn from the RMSE analysis.